Noname manuscript No.
(will be inserted by the editor)

Capturing composite waves in non-convex special relativistic hydrodynamics

Antonio Marquina · Susana Serna · José M. Ibáñez

Received: date / Accepted: date

Abstract We deal with the numerical approximation of the complex structure in special relativistic hydrodynamics (SRHD) when the system is closed with a non-convex equation of state (EOS). We consider a recently introduced phenomenological EOS ([20]) that mimics the loss of classical behavior when the fluid enters into a non-convex - thermodynamically - region in the relativistic regime. We introduce a flux formulation to approximate the solution of Riemann problems in SRHD such that the non-classical dynamics is detected and well resolved. We also design a strategy to recover primitive variables based on iterative procedures and present a detailed analysis providing a sufficient condition to ensure convergence. We propose a set of Riemann problems in one and two dimensions including blast waves, colliding slabs and expanding slabs, illustrating the strong complex dynamics arising in non-convex SRHD.

1 Introduction

The equations of special relativistic hydrodynamics (SRHD) form a nonlinear system of conservation laws [2, 26] which is closed with the constitutive relations represented by an equation of state (EOS) characterizing the equilibrium thermodynamic properties of the considered material. The thermodynamics, through the EOS, provides the classical or non-classical (convex or non-convex) character of the wave structure [31].

A. Marquina
Departamento Matemáticas, Universitat de València, Burjassot-València, Spain
E-mail: marquina@uv.es

S. Serna
Departament de Matemàtiques, Universitat Autònoma de Barcelona, Bellaterra-Barcelona, Spain
E-mail: serna@mat.uab.es

J. M. Ibáñez
Departamento de Astronomía y Astrofísica, Universitat de València, Burjassot-València, Spain
E-mail: jose.m.ibanez@uv.es

Since the pioneering works of [5], [47], and [41] the dynamics of non-convex fluids, i.e., those governed by a thermodynamics having a region of negative values of the fundamental derivative (see below), have drawn the attention of scientists working, mainly, in industrial applications (see, e.g., [13,42,7,8,14]). During their evolution non-convex flows can develop composite waves as, e.g., rarefaction shocks.

There are many astrophysical scenarios governed by relativistic (magneto-) hydrodynamical processes. A very outstanding example is the recent detection of GW170817, the gravitational wave signal coming from two colliding neutron stars [24]. The very rich and complex thermodynamics involved in such a system (a hypermassive neutron star, or a neutron star collapsing to form a black hole) is still an open problem for the community of nuclear physicists interested in the properties of dense matter. A necessary (not sufficient) condition for a non-convex thermodynamics is the non-monotonicity of the local speed of sound (or, closely related, the adiabatic index). Evidences of a non-monotonic behavior of the adiabatic index were already detected in some of the early EOSs derived from a field-theoretical model for nuclear and neutron matter [25]. In the light of the current knowledge on the properties of matter at high densities (greater than about $2\,10^{14}\,g/cm^3$) we can say that there are more evidences indicating that the local speed of sound is non-monotone [15–17,4]. In the Appendix C of the book [17] authors derive analytical representations of unified EOSs used in astrophysical applications; in particular, figure C2 (in that Appendix C) shows a fitting of the adiabatic index for the so-called SLy EOS - one of the most popular EOS used in hydrodynamical simulations of the above astrophysical scenarios - that displays, in some regions of the space of thermodynamical parameters, a Gaussian-like shape. A more recent analysis on the non-monotonicity of the local sound speed in many EOS for dense matter can be found in [1]. Motivated by these evidences we have proposed a phenomenological EOS in [20] that mimics the non-monotonic behaviour of the adiabatic index (see, also, figure 1 in [20]).

Traditionally, numerical schemes have been designed relying on the classical behavior of the wave structure (convexity of the system of equations) taking the ideal gas EOS as the model EOS. In this study we deal with the numerical approximation of the complex structure of SRHD when the system is closed with a non-convex EOS. We consider a recently introduced phenomenological EOS ([20]) that mimics the loss of classical behavior when the fluid enters into a non-convex - thermodynamically - region in the relativistic regime. We design a flux formulation approach to approximate the solution of Riemann problems in SRHD such that the non-classical dynamics is detected and well resolved. We also propose an iterative procedure to recover primitive variables ensuring convergence around the boundary of the non-convex region.

The evolution of a compressible fluid is described by a system of nonlinear conservation laws of the form

$$\frac{\partial \mathbf{u}}{\partial t} + \frac{\partial \mathbf{f}(\mathbf{u})}{\partial x} = 0 \tag{1}$$

where $\mathbf{u} = (u_1, \cdots, u_p)$ is the vector of conserved variables and $\mathbf{f}(\mathbf{u})$ is the vector of the fluxes. The system is closed with an EOS.

The behavior of the nonlinear characteristic wavefields is determined by the scalar quantity known as *nonlinearity factor*

$$\nu_k(\mathbf{u}) \equiv \nabla_{\mathbf{u}} \lambda_k(\mathbf{u}) \mathbf{r}_k(\mathbf{u}) \tag{2}$$

where $\lambda_k(\mathbf{u})$ and $\mathbf{r}_k(\mathbf{u})$ are the kth characteristic field eigenvalue and right eigenvector of the Jacobian $\mathbf{f}'(\mathbf{u})$. Positive values of $\nu_k(\mathbf{u})$ determine genuine nonlinearity of the wavefields and classical nonlinear wave structure as expansive rarefaction waves and compressive shocks [22]. Change of sign of the nonlinearity factor, $\nu_k(\mathbf{u})$, induces non-genuinely nonlinearity of the corresponding wavefields giving rise to the formation of complex (non-classical) wave structure of two types: it splits a shock in two parts and introduces between them a progressive wave or it splits a progressive wave and introduces a shock. Four different composite waves configurations can be obtained considering compression or expansion: double shocks separated by a compression fan, rarefaction shocks separated by an expansion fan, compression wave split by a shock and expansion fan split by a rarefaction shock [5,47,41].

In classical hydrodynamics described by Euler equations the nonlinearity factor $\nu_k(\mathbf{u})$ is proportional to the fundamental derivative, $\mathcal{G}$, a thermodynamical magnitude defined as

$$\mathcal{G} := -\frac{1}{2} V \frac{\left.\frac{\partial^2 P}{\partial V^2}\right|_s}{\left.\frac{\partial P}{\partial V}\right|_s} \tag{3}$$

where V is the specific volume, subindex s is the specific entropy and P is the pressure defined through an EOS. Therefore, changes of sign of $\mathcal{G}$ (non-convex - thermodynamically - region) determine the complexity of the wave structure in hydrodynamics. The thermodynamical magnitude $\mathcal{G}$ measures the convexity of isentropes in the $P-V$ plane, [32,41]. If $\mathcal{G} > 0$ the isentropes are convex and the classical dynamics is referred as convex as well as the EOS defining such pressure. Conversely, if $\mathcal{G}$ changes sign, the non-classical dynamics is characterized as non-convex as is the associated EOS.

In more complex systems of conservation laws, non-classical dynamics is not exclusively related to the thermodynamics through the change of sign of the fundamental derivative. In magnetohydrodynamics the loss of genuinely nonlinearity of the nonlinear wavefields, i.e., the change of sign of $\nu_k(\mathbf{u})$, is determined by both the thermodynamical properties of the material (through $\mathcal{G}$) and by the rotation of the magnetic field, [6,37,38]. In SRHD, Ibáñez et al. [19] proved that the nonlinearity factor is

$$\nu_k(\mathbf{u}) \propto \mathcal{G} - \frac{3}{2} c_s^2 \tag{4}$$

i.e., non-genuinely nonlinearity (non-classical behavior) may be induced not only by the thermodynamics associated to the EOS but also by relativistic effects through the relativistic speed of sound, c_s.

The accurate and robust numerical approximation of SRHD equations has been the focus of many authors [11,12,26,27,23,29,35,43,44]. However, to the best of our knowledge, none of these approaches have been specifically designed to capture complex wave structure induced by the loss of genuinely nonlinearity of the nonlinear wavefields. In this paper we present a numerical scheme to capture

the complex wave structure in SRHD when the system is closed with a non-convex EOS.

It has been shown in non-convex classical hydrodynamics and magnetohydrodynamics that in order to capture the complex wave structure in non-classical dynamics numerical schemes require an appropriate level of dissipation [3,6,13, 18,36–38]. However, prescribing too large numerical dissipation might prevent the formation of complex waves. In our approach for the case of non-convex SRHD we propose a characteristic based entropy-fix upwind strategy similarly as the one used for MHD [37,38]. The numerical scheme detects regions where non-convex dynamics arise and prescribes enough dissipation to capture the physically consistent solution.

On the other hand, as numerical schemes for the approximation of the solution SRHD equations need of a recovery algorithm to obtain the value of the pressure from the updated conserved variables in each time step, we analyze the influence of the induced non convex dynamics in this recovery procedure. We characterize the convergence of classical iterative methods for recovering primitive variables in terms of the fundamental derivative. We propose a strategy for the iterative process of recovering primitive variables in the presence of non-convex - thermodynamically - regions and prove that convergence is ensured by choosing a nonnegative initial guess.

In order to follow this study we consider the phenomenological non-convex EOS presented in [20] as a simple model exhibiting the complex wave behavior caused by loss of genuinely nonlinearity of the nonlinear wave fields. The EOS is proved to induce nonclassical dynamics because of pure thermodynamic effects as $\mathcal{G}$ becomes negative and by genuine relativistic effects, ie, $\mathcal{G}-\frac{3}{2}c_s^2<0$ while $\mathcal{G}>0$.

Finally we propose a set of Riemann problems to illustrate the strong complex dynamics of SRHD systems closed with a non-convex EOS.

The paper is organized as follows. In section 2 we analyze the non-convex EOS and establish the necessary conditions to ensure hyperbolicity of the system of SRHD equations closed with such EOS. Section 3 is dedicated to the numerical approximation of general SRHD system of equations. We propose a flux formulation for solving non-convex SRHD and a strategy to recover primitive variables with a detailed analysis providing a sufficient condition to ensure convergence. We present the numerical approximation of the evolution of a set of Riemann problems in Section 4. We draw our conclusions in Section 5.

2 A phenomenological non-convex equation of state

The one dimensional system of special relativistic hydrodynamics (SRHD) equations is a system of hyperbolic conservation laws

$$\frac{\partial D}{\partial t}+\frac{\partial}{\partial x}(Dv)=0 \tag{5}$$

$$\frac{\partial S}{\partial t}+\frac{\partial}{\partial x}(Sv+P)=0 \tag{6}$$

$$\frac{\partial \tau}{\partial t}+\frac{\partial}{\partial x}(S-Dv)=0 \tag{7}$$

where the conserved variables, D, S and τ, rest-mass density, momentum density and energy density respectively, are defined as

$$D = \rho W \tag{8}$$
$$S = \rho h W^2 v \tag{9}$$
$$\tau = \rho h W^2 - P - D \tag{10}$$

being v the velocity (in units of the speed of light), ρ the density and P the pressure, [26]. The system is closed with an EOS, $P = P(\rho, \epsilon)$ (ϵ, the specific internal energy), defining the thermodynamic properties of the material. Note that P, ρ and v, known as *primitive* variables, are not explicit functions of the conserved variables D, S and τ. W is the Lorentz factor

$$W = \frac{1}{\sqrt{1 - v^2}} \tag{11}$$

and h the specific (relativistic) enthalpy

$$h = 1 + \epsilon + \frac{P}{\rho} \tag{12}$$

In this section we establish the necessary conditions to ensure hyperbolicity of the system of SRHD equations (5-7) when the system is closed with a non-convex phenomenological EOS for relativistic flows as the one introduced in [20].

The phenomenological EOS proposed in [20], named GGL ('Gaussian Gamma Law'), is a model EOS that mimics the anomalies caused by loss of convexity of isentropes in the $P-V$ plane in relativistic scenarios. It can be written resembling a Mie-Grüneisen EOS, ([31])

$$P(\rho, \epsilon) = \Gamma(\rho)\rho\epsilon \tag{13}$$

where the Grüneisen coefficient is defined as

$$\Gamma(\rho) = \gamma(\rho) - 1 \tag{14}$$

and

$$\gamma(\rho) = \gamma_0 + (\gamma_1 - \gamma_0)\, \exp\left(-\frac{(\rho - \rho_1)^2}{\sigma^2}\right) \tag{15}$$

$$\gamma_1 = \gamma(\rho_1), 1 < \frac{4}{3} \leq \gamma_0 < \gamma_1 < 2 \tag{16}$$

being $\sigma > 0$ and $\rho_1 > 0$ parameters playing the role of a simple scale factor for the density. There are four free parameters defining the EOS: $\gamma_0, \gamma_1, \rho_1, \sigma$. The phenomenological EOS can be extended to a complete EOS defining a temperature and an entropy functions from $\Gamma(\rho)$ ([31]).

Given an EOS there are three thermodynamical magnitudes playing an important role in the dynamics of SRHD: the relativistic enthalpy (12), the relativistic speed of sound

$$c_s^2 = \frac{1}{h}\frac{\partial P}{\partial \rho}\Big|_s \tag{17}$$

where subindex s represents the entropy and the fundamental derivative $\mathcal{G}$, (3), defining the regions of change of convexity of isentropes in the $P-V$ plane .

For the EOS (13-16), the relativistic enthalpy and the square of the relativistic speed of sound become respectively

$$h(\rho,\epsilon) = 1 + \gamma(\rho)\epsilon \tag{18}$$

and

$$c_s^2(\rho,\epsilon) = \frac{1}{h}\frac{\partial P}{\partial \rho}\Big|_s = \frac{1}{h}\Big(\frac{\partial P}{\partial \rho} + \frac{P}{\rho^2}\frac{\partial P}{\partial \epsilon}\Big) = \frac{\epsilon}{h}\Big(\gamma(\rho)(\gamma(\rho)-1) + \rho\gamma'(\rho)\Big) \tag{19}$$

Alternatively, we can rewrite (19) as:

$$c_s^2(\rho,\epsilon) \;=\; \frac{\gamma(\rho)\epsilon}{h}\left(\gamma(\rho) - 1 + \frac{d\,ln\,\gamma}{d\,ln\,\rho}\right), \tag{20}$$

where the term between parenthesis on the right hand side in (20) satisfies the following asymptotic relationship:

$$\lim_{\epsilon\to\infty} c_s^2 \;=\; \gamma - 1 + \frac{dln\gamma}{dln\rho} \tag{21}$$

The corresponding expression of the fundamental derivative becomes

$$\mathcal{G}(\rho) = \frac{1+\gamma(\rho)}{2} + \frac{\rho}{2}\frac{2\gamma(\rho)\gamma'(\rho) + \rho\gamma''(\rho)}{\gamma(\rho)(\gamma(\rho)-1) + \rho\gamma'(\rho)} \tag{22}$$

where

$$\gamma'(\rho) = -\frac{2(\gamma_1-\gamma_0)(\rho-\rho_1)}{\sigma^2}\exp\left(-\frac{(\rho-\rho_1)^2}{\sigma^2}\right) \tag{23}$$

$$\gamma''(\rho) = \left(\frac{2(\rho-\rho_1)^2}{\sigma^2} - 1\right)\frac{2(\gamma_1-\gamma_0)}{\sigma^2}\exp\left(-\frac{(\rho-\rho_1)^2}{\sigma^2}\right) \tag{24}$$

As seen in [20] the fundamental derivative $\mathcal{G}(\rho)$ changes sign for specific set of parameters inducing non-classical dynamics.

The hyperbolicity of the SRHD equations is guaranteed for those EOSs satisfying two conditions namely: thermodynamical consistency, $c_s^2 \geq 0$, and causality, $c_s^2 < 1$, [2]. By construction, our GGL-EOS is consistent and causal in both limits at high and low densities. However, in the narrow region around ρ_1, $]0, \rho_1 + 2\sigma]$, these properties can fail. In the following propositions we determine the requisites under which the phenomenological EOS (13-16) satisfies those constraints in $]0, \rho_1 + 2\sigma]$.

Proposition 1 *Given a phenomenological EOS defined through (13-16) the following conditions are equivalent*

1. *The speed of sound satisfies $c_s^2 \geq 0, \forall\rho,\epsilon$, (i.e., the EOS is thermodynamically consistent)*
2. $$\gamma(\rho)(\gamma(\rho)-1) + \rho\gamma'(\rho) \geq 0, \qquad \forall\rho \in]0,\infty[\tag{25}$$

3.

$$\gamma(\rho)(\gamma(\rho)-1)+\rho\gamma'(\rho)\geq 0, \qquad \forall\rho\in]0,\rho_1+2\sigma] \tag{26}$$

Proof:
(*1*) $\leftrightarrow$ (*2*) From the definition of c_s^2 in (19), since $h(\rho,\epsilon)>0$ and $\epsilon>0$ everywhere, it is clear that (*1*) and (*2*) are equivalent.
(*2*) $\rightarrow$ (*3*) It is obvious.
(*3*) $\rightarrow$ (*2*) Let us introduce a new variable $x=\frac{\rho}{\sigma}$. We set $x_1=\frac{\rho_1}{\sigma}$ and, for $\rho=\sigma x$ we define

$$G(x)=\gamma(\sigma x)(\gamma(\sigma x)-1)+\sigma x\gamma'(\sigma x)$$

which can be rewritten as

$$G(x)=g(x)(g(x)-1)+xg'(x)$$

with $g(x)=\gamma(\sigma x)$.

In this context the hypothesis can be written as

$$G(x)\geq 0,\ \ \forall\, x\in]0,x_1+2]$$

We then need to prove that $G(x)\geq 0,\ \ \forall\, x>x_1+2$.

We have that $G'(x)=2g(x)g'(x)+xg''(x)$ with

$$g'(x)=-2(\gamma_1-\gamma_0)\exp(-(x-x_1)^2)(x-x_1)$$

and $g''(x)=2(\gamma_1-\gamma_0)\exp(-(x-x_1)^2)(2(x-x_1)^2-1)$.

Let $a\geq 2$ any real number. Then,

$$G'(x_1+a)=2(\gamma_1-\gamma_0)\exp(-a^2)(2a^3+(2a^2-1)x_1-a(1+2g(x_1+a)))$$

Because of $1<g(x_1+a)\leq 2$ and $a\geq 2$ we have that $G'(x_1+a)>0$ for all $a\geq 2$. Then $G(x)$ is strictly increasing for $x\geq x_1+2$ and

$$G(x)\geq G(x_1+2)\geq 0,\ \ \forall x\geq x_1+2$$

Therefore,

$$\gamma(\rho)(\gamma(\rho)-1)+\rho\gamma'(\rho)\geq 0, \qquad \forall\rho\geq\rho_1+2\sigma$$

and, by (19), $c_s^2\geq 0\ \forall\rho$. □

Proposition 2 *Given a phenomenological EOS of type (13-16) which is thermodynamically consistent ($c_s^2\geq 0$), then the following conditions are equivalent:*

1. *The EOS is causal, i.e., $c_s^2<1,\ \forall\rho,\epsilon$.*
2. $$\gamma(\rho)(2-\gamma(\rho))-\rho\gamma'(\rho)>0, \qquad \forall\rho\in]0,\infty[\tag{27}$$
3. $$\gamma(\rho)(2-\gamma(\rho))-\rho\gamma'(\rho)>0, \qquad \forall\rho\in]0,\rho_1+2\sigma] \tag{28}$$

Proof:
(1) $\rightarrow$ *(2)* Let us assume first that $0 \leq c_s^2 < 1$ for all $\rho > 0$ and $\epsilon > 0$. From the expression of c_s^2, (19), we have

$$0 \leq \frac{\epsilon}{h}\Big(\gamma(\rho)(\gamma(\rho)-1) + \rho\gamma'(\rho)\Big) < 1$$

Since $\epsilon > 0$, we have from (18) that $h > 0$ and then

$$h > \epsilon\Big(\gamma(\rho)(\gamma(\rho)-1) + \rho\gamma'(\rho)\Big) \geq 0, \qquad \forall \rho > 0$$

Using (18) we obtain

$$1 + \gamma(\rho)\epsilon > \epsilon\Big(\gamma(\rho)(\gamma(\rho)-1) + \rho\gamma'(\rho)\Big).$$

Thus,

$$1 + \epsilon(\gamma(\rho)(2-\gamma(\rho)) - \rho\gamma'(\rho)) > 0, \qquad \forall \rho > 0, \epsilon > 0.$$

Because of $\epsilon > 0$, is independent of ρ and arbitrarily large, we have

$$\gamma(\rho)(2-\gamma(\rho)) - \rho\gamma'(\rho) > 0, \qquad \forall \rho.$$

(2) $\rightarrow$ *(1)* The above reasoning is reversible to prove this statement.
(2) $\leftrightarrow$ *(3)* Assuming (26) the inequality (28) holds also for all $\rho > 0$ because from (23) we have that for $\rho \geq \rho_1$, $\gamma'(\rho) < 0$. $\square$

We propose two sets of parameters in Table 1 to define two examples of phenomenological EOS with non-convex behavior. The parameters are chosen such that both EOSs are thermodynamically consistent and causal. Indeed, left and right pictures in Figure 1 for EOS 1 and EOS2 respectively, show real functions of ρ of expressions in (26) and (28) represented over an interval containing $]0, \rho_1 + 2\sigma]$ as determined in Propositions 1 and 2. We observe that both functions are strictly positive implying that both EOSs are thermodynamically consistent and causal.

In Figure 2 we represent the value of the fundamental derivative for each EOS in a neighborhood of ρ_1. We observe that $\mathcal{G}$ changes sign and shows the largest variation in this region. Both EOS are therefore non-convex and will induce nonclassical wave dynamics.

The value of $\gamma_1 = 1.9$ has been taken from the studies of hydrodynamical supernovae (or core-collapse supernovae, CC-SN). During the gravitational collapse (infall epoch) of the iron core inside a massive progenitor star, at the latest stages of its evolution, the adiabatic index changes abruptly from $\approx 4/3$ to ≈ 2. This dramatic change drives an initial strong shock (bounce epoch) that can lead to the explosion in the so-called prompt mechanism, the most basic piece or ingredient of the complex theory of CC-SN (see, e.g., the review [21]). The value of $\gamma_1 = 5/3$ has been taken just for the sake of comparison.

Table 1 EOS parameters

Model	ρ_1	γ_0	γ_1	σ
EOS1	1	4/3	5/3	0.6
EOS2	1	4/3	1.9	1.1

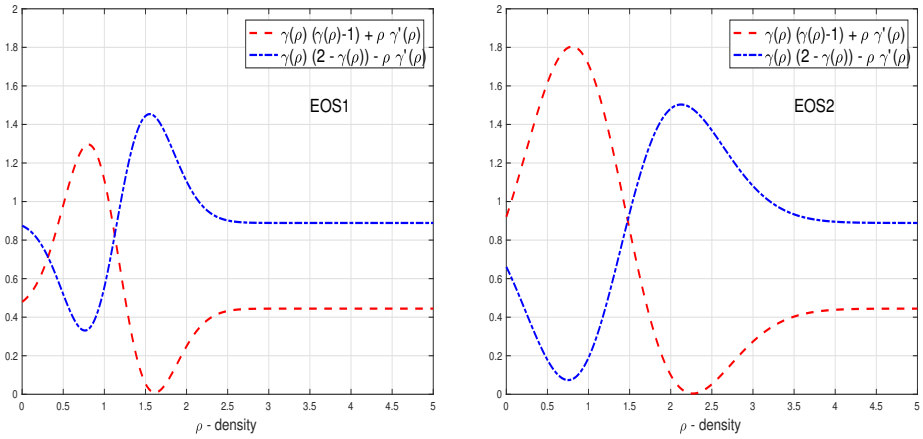

Fig. 1 Evidence of causality and thermodynamic consistency for EOS1 and EOS2

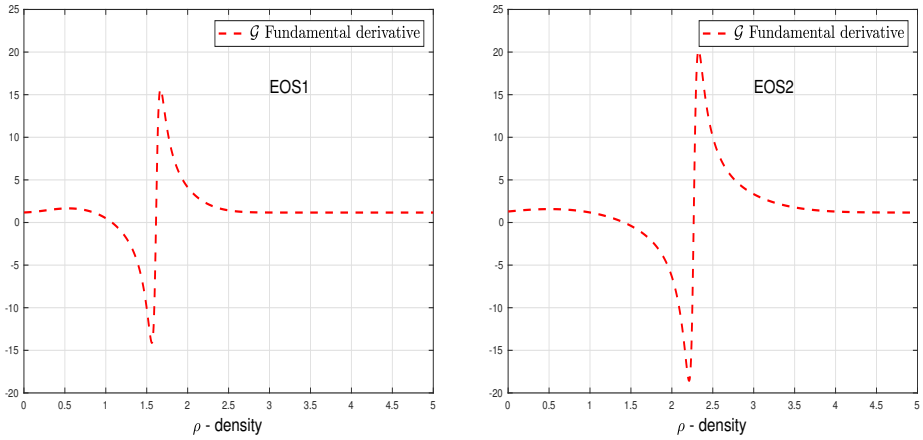

Fig. 2 Fundamental derivative for EOS1 and EOS2

3 Numerical approximation of general SRHD

The numerical approximation of the solution of the SRHD system of equations is a challenging task. The ultrarelativistic regime is known because of the extremely strong shock structures appearing in the dynamics. The equations are strongly coupled through the Lorentz factor, W, and the relativistic enthalpy, h, bringing up a very nonlinear wave interaction [11, 12, 23, 26, 28, 35]. Moreover conserved and primitive variables are related through a set of non-linear equations that need to be solved in each point at every time step.

Any numerical scheme to solve the system of SRHD equations is composed of two main algorithms. A flux formula to solve the nonlinear coupled equations and an iterative procedure to recover primitive variables, i.e., to accurately calculate, in each cell and every time step, the pressure and other primitive variables from the conserved ones.

We consider the system of SRHD equations (5-7) closed with a non-convex EOS that induces non-classical dynamics. The complexity of the wave structure is determined by the nonlinear wavefields through the nonlinearity term (2), that in SRHD adopts the form ([19]),

$$\nu(\rho,\epsilon)=\frac{c_s}{\rho}\Big(\mathcal{G}-\frac{3}{2}c_s^2\Big) \tag{29}$$

There exist hyperbolic singularities when the nonlinearity term changes sign inducing non-convex (non-classical) dynamics showing the formation of complex wave structure. The loss of genuinely nonlinearity of the nonlinear wavefields may be caused because of the existence of a non-convex - thermodynamically - region there where $\mathcal{G}$ changes sign or because of genuine non-convex relativistic effects when $\nu(\rho,\epsilon)\leq 0$ while $\mathcal{G}>0$.

We propose a numerical scheme to approximate the solution of general SRHD closed with a non-convex EOS where complex wave structure arises as a consequence of the existence of a non-convex - thermodynamically - region due to genuine non-convex relativistic effects. The numerical scheme consists of a flux formulation based on a Riemann solver that resolves the wave dynamics by local characteristic wavefields. The flux formulation is able to identify local regions containing non-convex singularities and to introduce a local viscosity ensuring convergence to the entropy solution. Two iterative procedures for the recovery of the primitive variables, fixed-point and Newton's iterations, are presented and their convergence is analyzed in terms of the relativistic speed of sound. In particular we prove that the quadratic convergence of Newton's method is compromised by the thermodynamics through the magnitude of $\mathcal{G}$.

3.1 A flux formula for solving non-convex SRHD equations

In order to capture the admissible solution of the system of equations and resolve the complex wave structure appearing in the dynamics as a consequence of the nonlinear wave interaction, a numerical scheme must prescribe a certain level of dissipation. Numerical schemes prescribing global viscosity ensure stability and computational efficiency, yet overmuch dissipation causes loss of accuracy, blurring of fine structure and the risk of preventing the formation of complex waves. The most common ways to overcome the excess of dissipation involve high order versions of the basic scheme or the use of very fine grids.

We consider a one dimensional numerical scheme in conservation form in one dimension written as

$$\mathbf{u}_j^{n+1}=\mathbf{u}_j^n-\frac{\Delta t}{\Delta x}\big(\tilde{\mathbf{f}}_{j+\frac{1}{2}}-\tilde{\mathbf{f}}_{j-\frac{1}{2}}\big) \tag{30}$$

where $\mathbf{u}_j^n\approx\mathbf{u}(x_j,t_n)$ is a numerical approximation of the solution in the computational cell and $x_j=x_0+j\Delta x$, $t_n=n\Delta t$ where Δx and Δt are the spatial and

time step sizes respectively. The numerical flux $\tilde{\mathbf{f}}_{j+\frac{1}{2}}$ is a function of $2k$ variables $\tilde{\mathbf{f}}_{j+\frac{1}{2}} = \tilde{\mathbf{f}}(u_{j-k+1}, \cdots, u_{j+k})$ that is consistent with (1).

With the goal of using a low dissipative numerical scheme we propose a characteristic based upwind approach to solve the wave dynamics of non-convex SRHD.

The numerical characteristic fluxes are computed following a similar manner as proposed for general magnetohydrodynamics ([38]). From the local characteristic structure the numerical scheme detects regions where non-convex dynamics arise and prescribes enough dissipation to capture the physically consistent solution. We consider three types of interfaces namely: *singular, sonic* and *upwind*. Singular interfaces are those containing points of non-convex hyperbolicity, i.e., isolated points where the nonlinearity factor (29) vanishes. A sonic interface is an interface where the characteristic wave speeds (eigenvalues of the Jacobian of the fluxes) change sign, i.e., there is at least one $p \in \{1, 2, 3\}$ such that $\lambda_p(\mathbf{u}_j^n) \cdot \lambda_p(\mathbf{u}_{j+1}^n) < 0$. An upwind interface is an interface that is neither singular nor sonic.

We solve the local characteristic fields using the upwind choice at upwind interfaces. The upwind scheme is defined according to the sign of the local wave velocities approximating at the interface with very low dissipation. Because of the lack of dissipation, the upwind approach is non monotone in regions where new structure is generated as a result of the nonlinear wave interaction and fails to converge to the entropy solution around sonic and singular interfaces. Transonic rarefaction waves around sonic interfaces and composite waves in regions of negativity of the nonlinear term, are not well resolved by the upwind strategy. Waves must admit viscous profiles and the scheme has to provide an appropriate level of dissipation to allow the formation of the physical solution. In non upwind interfaces we solve the local characteristic fields by a Lax-Friedrichs procedure prescribing an appropriate viscosity that is consistent with the equations. This is done locally in space and time over all characteristic fields around sonic and singular interfaces. The procedure is as follows.

The first step consists of calculating the complete system of eigenvectors, $\mathbf{r}$ and $\mathbf{l}$, at $\mathbf{u}_j^n$ and $\mathbf{u}_{j+1}^n$ and the associated eigenvalues $\lambda_p(\mathbf{u}_j^n)$ and $\lambda_p(\mathbf{u}_{j+1}^n)$ for $p = 1, 2, 3$ of the Jacobian of the fluxes $\mathbf{f}'(\mathbf{u})$ following the spectral decomposition derived in [11]. The eigenvalues of the Jacobian are

$$\lambda_1 = \frac{v - c_s}{1 - v c_s}; \qquad \lambda_2 = v; \qquad \lambda_3 = \frac{v + c_s}{1 + v c_s}$$

Let us define $\mathcal{K} = \dfrac{\Gamma}{\Gamma - c_s^2}$ where $\Gamma = \dfrac{1}{\rho}\dfrac{\partial P}{\partial \epsilon}$ is the Grüneisen coefficient ($\Gamma = \gamma(\rho) - 1$ for our phenomenological GGL-EOS).

Then, the right eigenvectors are

$$\mathbf{r}_{1,3}(\mathbf{u}) = \Big(1, hW(v \mp c_s), hW(1 \mp v c_s) - 1\Big)$$
$$\mathbf{r}_2(\mathbf{u}) = \Big(\frac{\mathcal{K}}{hW}, v, 1 - \frac{\mathcal{K}}{hW}\Big)$$

and the left eigenvectors

$$\mathbf{l}_{1,3}(\mathbf{u}) = \pm\frac{h^2}{\Delta}\Big(\mathcal{K}(v \mp c_s) - v \pm hW c_s(1 - v^2), 1 - \mathcal{K}(1 \mp v c_s), \mathcal{K}(v \mp c_s) - v\Big)$$
$$\mathbf{l}_2(\mathbf{u}) = \frac{W}{\mathcal{K} - 1}\Big(h - W, Wv, -W\Big)$$

where $\Delta := h^3 W(\mathcal{K}-1)(1-v^2)2c_s$.

The first order accurate approximation of the system of equations has the form

$$\mathbf{u}_j^{n+1} = \mathbf{u}_j^n - \frac{\Delta t}{\Delta x}\left(\tilde{\mathbf{f}}(\mathbf{u}_j^n, \mathbf{u}_{j+1}^n) - \tilde{\mathbf{f}}(\mathbf{u}_{j-1}^n, \mathbf{u}_j^n)\right)$$

such that $\tilde{\mathbf{f}}(\mathbf{u}, \mathbf{u}) = \mathbf{f}(\mathbf{u})$.

We compute the numerical flux $\tilde{\mathbf{f}}(\mathbf{u})$ in terms of two linearizations, one at each side of the interface $j+\frac{1}{2}$ following Marquina's flux splitting strategy [10]. The flux formulation has been proved to behave robust in multiple scenarios [11,36–38].The calculation of the numerical flux corresponding to the cell-interface separating the states $\mathbf{u}_j^n$ and $\mathbf{u}_{j+1}^n$ is done by

$$\tilde{\mathbf{f}}(\mathbf{u}_j^n, \mathbf{u}_{j+1}^n) = \sum_{p=1}^{3}\left[\psi_+^p \mathbf{r}_p(\mathbf{u}_j^n) + \psi_-^p \mathbf{r}_p^f(\mathbf{u}_{j+1}^n)\right] \tag{31}$$

where ψ_+^p and ψ_-^p represent the lateral numerical characteristic fluxes at the interface. These are all obtained as functions of the local characteristic fluxes and variables but differently depending on the nature of the interface.

The local characteristic fluxes and variables are calculated by the scalar product of the fluxes and the left eigenvectors at both sides of the interface as

$$\begin{aligned} \phi_j^p &= \mathbf{f}(\mathbf{u}_j^n)\cdot\mathbf{l}_p(\mathbf{u}_j^n) \qquad & \phi_{j+1}^p &= \mathbf{f}(\mathbf{u}_{j+1}^n)\cdot\mathbf{l}_p(\mathbf{u}_{j+1}^n) \\ w_j^p &= \mathbf{u}_j^n\cdot\mathbf{l}_p(\mathbf{u}_j^n) & w_{j+1}^p &= \mathbf{u}_{j+1}^n\cdot\mathbf{l}_p(\mathbf{u}_{j+1}^n) \end{aligned}$$

for $p = 1, 2, 3$.

A first order approximation of the numerical characteristic fluxes ψ_+^p and ψ_-^p in (31) is determined at both sides of the interface from the following procedure.

for $j = 1, \cdots, n$

if $\nu_1(\mathbf{u})$ or $\nu_3(\mathbf{u})$ change sign (**singular interface**)

$\alpha_c = \max(|\lambda_p(\mathbf{u}_j^n)|, |\lambda_p(\mathbf{u}_{j+1}^n)|), \quad p = 1, 2, 3$

$\alpha_s = \frac{1}{2}\sqrt{\alpha_c^2 + 1}$ (as the speed of light is scaled to 1)

$\psi_+^p = \frac{1}{2}(\phi_j^p + \alpha_s w_j^p); \qquad \psi_-^p = \frac{1}{2}(\phi_{j+1}^p - \alpha_s w_{j+1}^p); \qquad p = 1, 2, 3$

else

if $\lambda_p(\mathbf{u}_j^n)\cdot\lambda_p(\mathbf{u}_{j+1}^n) > 0, \ \forall p = 1, 2, 3$, (**upwind interface**)

if $\lambda_p(\mathbf{u}_j^n) > 0$,

$\psi_+^p = \phi_j^p; \qquad \psi_-^p = 0 \qquad p = 1, 2, 3$

else

$\psi_+^p = 0; \qquad \psi_-^p = \phi_{j+1}^p \qquad p = 1, 2, 3$

endif

else (**sonic interface**)

$\alpha_c = \max(|\lambda_p(\mathbf{u}_j^n)|, |\lambda_p(\mathbf{u}_{j+1}^n)|), \qquad p = 1, 2, 3$

$\psi_+^p = \frac{1}{2}(\phi_j^p + \alpha_c w_j^p); \qquad \psi_-^p = \frac{1}{2}(\phi_{j+1}^p - \alpha_c w_{j+1}^p); \qquad p = 1, 2, 3$

endif

endif

end

The proposed numerical method is stable under a Courant-Friedrichs-Lewy (CFL) condition ([22]) determined by

$$\Delta t = C\frac{\Delta x}{\max(\max_{\mathbf{u}}|\lambda_1(\mathbf{u})|, \max_{\mathbf{u}}|\lambda_3(\mathbf{u})|)}, \qquad 0 < C < 1 \tag{32}$$

In practice the upper bound of the characteristic speeds, 1, can be used instead of $\max(\max_{\mathbf{u}}|\lambda_1(\mathbf{u})|, \max_{\mathbf{u}}|\lambda_3(\mathbf{u})|)$.

We implement the above algorithm to high order accuracy. We follow the Shu-Osher approach ([39]) by applying a reconstruction procedure on local characteristic fluxes and variables. We use the piecewise hyperbolic method (PHM) (three point stencil) as reconstruction procedure to achieve third order accuracy in space [30].

The Marquina's flux splitting strategy implemented to high order accuracy in space is as follows.Two linearizations at each interface are considered

$$\mathbf{u}_j^{n+1} = \mathbf{u}_j^n - \frac{\Delta t}{\Delta x}\big(\tilde{\mathbf{f}}(\mathbf{u}_{j+\frac{1}{2}}^{n,L}, \mathbf{u}_{j+\frac{1}{2}}^{n,R}) - \tilde{\mathbf{f}}(\mathbf{u}_{j-\frac{1}{2}}^{n,L}, \mathbf{u}_{j-\frac{1}{2}}^{n,R}))\big)$$

where

$$\tilde{\mathbf{f}}(\mathbf{u}_{j+\frac{1}{2}}^{n,L}, \mathbf{u}_{j+\frac{1}{2}}^{n,R}) = \sum_{p=1}^{3}\Big[\psi_{j+\frac{1}{2}}^{L}\mathbf{r}_p^f(\mathbf{u}_{j+\frac{1}{2}}^{L}) + \psi_{j+\frac{1}{2}}^{R}\mathbf{r}_p^f(\mathbf{u}_{j+\frac{1}{2}}^{R})\Big]$$

The high order numerical characteristic fluxes $\psi_{j+\frac{1}{2}}^{L} = (\psi_p^L)_{p=1}^3, \psi_{j+\frac{1}{2}}^{R} = (\psi_p^R)_{p=1}^3$ are obtained from high order accurate values of the local characteristic fluxes and variables following a similar procedure as mentioned previously for first order approximation.

for $j = 1, \cdots, n$

if $\nu_1(\mathbf{u})$ or $\nu_3(\mathbf{u})$ change sign (**singular interface**)

$\alpha_c = \max(|\lambda_p(\mathbf{u}_{j+\frac{1}{2}}^{L})|, |\lambda_p(\mathbf{u}_{j+\frac{1}{2}}^{R})|, \qquad p = 1, 2, 3$

$\alpha_s = \frac{1}{2}\sqrt{\alpha_c^2 + 1}$ (as the speed of light is scaled to 1)

$\psi_p^L = \frac{1}{2}(\phi_{j+\frac{1}{2}}^{L} - \alpha_s w_{j+\frac{1}{2}}^{L}) \qquad \psi_p^R = \frac{1}{2}(\phi_{j+\frac{1}{2}}^{R} + \alpha_s w_{j+\frac{1}{2}}^{R}) \qquad p = 1, 2, 3$

else

if $\lambda_p(\mathbf{u}_{j+\frac{1}{2}}^{L})\dot{\lambda}_p(\mathbf{u}_{j+\frac{1}{2}}^{R}) > 0\ \forall p = 1, 2, 3$, (**upwind interface**)

if $\lambda_p(\mathbf{u}_{j+\frac{1}{2}}^{L}) > 0$,

$\psi_p^L = \phi_{j+\frac{1}{2}}^{L}(p), \qquad \psi_p^R = 0$

else

$\psi_p^L = 0, \qquad \psi_p^R = \phi_{j+\frac{1}{2}}^{R}(p) \qquad p = 1, 2, 3$

endif

else (**sonic interface**)

$$\alpha_c = \max(|\lambda_p(\mathbf{u}^L_{j+\frac{1}{2}})|, |\lambda_p(\mathbf{u}^R_{j+\frac{1}{2}})|, \qquad p = 1,2,3$$

$$\psi^L_p = \frac{1}{2}(\phi^L_{j+\frac{1}{2}} - \alpha_c w^L_{j+\frac{1}{2}}); \qquad \psi^R_p = \frac{1}{2}(\phi^R_{j+\frac{1}{2}} + \alpha_c w^R_{j+\frac{1}{2}}) \qquad p = 1,2,3$$

endif

endif

end

In order to run this algorithm we previously need to evaluate the eigenvalues and eigenvectors and calculate the characteristic variables and fluxes at each side of the interface.

The approximate values of $\mathbf{u}$ at the interface from left and from right are obtained via a reconstruction procedure. In our case we use the PHM procedure that uses three points stencil

$\mathbf{u}^L_{j+\frac{1}{2}}$ =PHM$[\mathbf{u}^n_{j-1}, \mathbf{u}^n_j, \mathbf{u}^n_{j+1}]$; $\mathbf{u}^R_{j+\frac{1}{2}}$ =PHM$[\mathbf{u}^n_j, \mathbf{u}^n_{j+1}, \mathbf{u}^n_{j+2}]$

From these approximations, the eigenvalues and eigenvectors can be evaluated $\mathbf{l}(\mathbf{u}^L_{j+\frac{1}{2}})$, $\mathbf{l}(\mathbf{u}^R_{j+\frac{1}{2}})$, $\mathbf{r}(\mathbf{u}^L_{j+\frac{1}{2}})$, $\mathbf{r}(\mathbf{u}^R_{j+\frac{1}{2}})$, $\lambda_p(\mathbf{u}^L_{j+\frac{1}{2}})$, $\lambda_p(\mathbf{u}^R_{j+\frac{1}{2}})$ and the characteristic variables and fluxes calculated as

$w^L_k = \mathbf{l}(\mathbf{u}^L_{j+\frac{1}{2}})u^n_k, \qquad k = j-1, j, j+1$

$\phi^L_k = \mathbf{l}(\mathbf{u}^L_{j+\frac{1}{2}})\mathbf{f}(\mathbf{u}^n_k), \qquad k = j-1, j, j+1$

$w^R_k = \mathbf{l}(\mathbf{u}^R_{j+\frac{1}{2}})u^n_k, \qquad k = j, j+1, j+2$

$\phi^R_k = \mathbf{l}(\mathbf{u}^R_{j+\frac{1}{2}})\mathbf{f}(\mathbf{u}^n_k), \qquad k = j, j+1, j+2$

The high order characteristic variables and fluxes at interfaces are then obtained from

$w^L_{j+\frac{1}{2}}$=PHM$[w^L_{j-1}, w^L_j, w^L_{j+1}]$; $\phi^L_{j+\frac{1}{2}}$=PHM$[\phi^L_{j-1}, \phi^L_j, \phi^L_{j+1}]$

$w^R_{j+\frac{1}{2}}$=PHM$[w^R_j, w^R_{j+1}, w^R_{j+2}]$; $\phi^R_{j+\frac{1}{2}}$=PHM$[\phi^R_j, \phi^R_{j+1}, \phi^R_{j+2}]$

For the integration in time we utilize the third order accurate total variation diminishing Runge-Kutta time stepping procedure proposed in [39]. The extension to high order accuracy in space and time is proved to perform satisfactorily in resolving a set of one dimensional Riemann problems.

3.2 Recovering primitive variables

The calculus of the conserved variables in each time step is explicit following relations (5-7). However, this is not the case to compute the value of the pressure and the primitive variables ρ, v and ϵ. The use of an algorithm that calculates P and, eventually, the values of ρ, v and ϵ, from the updated admissible conserved variables D, S, τ, is required.

In this section we study two iterative procedures based on fixed-point and Newton methods to recover primitive variables in each time step of the evolution of SRHD equations. We analyze the domain and conditions of convergence for both methods when the system of SRHD equations is closed with a phenomenological EOS of type (13-16). We finalize proposing a methodology that combines both iterative methods as an efficient strategy to ensure convergence in the presence of strong and non-convex dynamics.

3.2.1 Fixed-point iterative method

We define a fixed-point iterative procedure using relations (8-10) to obtain successive approximations of the pressure starting from an initial pivot representing an estimated value of the pressure.

Definition 1 Let

$$x^{k+1} = F(x^k), \qquad k = 0, 1, \cdots \tag{33}$$

be a fixed-point iteration starting with $x^0 > 0$ (estimated value of the pressure at a specific time-step) where $F(x)$ is

$$F(x) := P(\rho(x), \epsilon(x)) \tag{34}$$

and

$$W(x) = \frac{1}{\sqrt{1 - \dfrac{S^2}{(\tau + x + D)^2}}} \tag{35}$$

$$\rho(x) = \frac{D}{W(x)} \tag{36}$$

$$\epsilon(x) = \frac{\tau + x + D}{DW(x)} - \frac{xW(x)}{D} - 1 \tag{37}$$

being D, S, τ constant values of the conserved variables provided at a specific time step of the evolution. We call $\rho(x), \epsilon(x)$ and $W(x)$ extended variables to x of ρ, ϵ and W respectively.

Each iteration x^k is a value representing an estimate of the pressure, P.

Definition 2 Let $D > 0, S, \tau > 0$ be a triple of conserved variables. We define the set of possible candidates for pressure values as

$$\mathcal{P}_{(D,S,\tau)} = \left\{ x > 0 : \frac{|S|}{\tau + x + D} < 1, \epsilon(x) > 0,\ 0 \le c_s^2(x) < 1 \right\}$$

Definition 3 A triple D, S, τ is a physically admissible set of conserved variables if there exist $P \in \mathcal{P}_{(D,S,\tau)}$ such that $F(P) = P$.

In the following we study the conditions under which the proposed fixed-point iteration is well defined and converges accurately to the pressure associated to the phenomenological EOS. In order to do so we validate the iterative procedure by verifying the conditions of the *fixed-point Theorem* ([34]).

Fixed-point Theorem *Let F be a continuous and differentiable function in $[a, b]$ satisfying*

(i) $F([a, b]) \subset [a, b]$,
(ii) $|F'(x)| \le \mu$ *for all* $x \in [a, b]$ *and for certain* $\mu < 1$.

Then function F has a unique fixed point (a point α for which $F(\alpha) = \alpha$) and for all $x_0 \in [a, b]$ the sequence $x^{k+1} = F(x^k)$ converges to α.

Conditions on the convergence of the fixed-point iterative method are given in terms of the derivative of the iteration function $F(x)$. Next proposition provides an expression of its derivative.

Proposition 3 *$F(x)$ is differentiable and the derivative can be expressed as*

$$\frac{dF}{dx} = v^2(x)c_s^2(x)$$

where $v^2(x)$ is the extension to x of v^2 (calculated from $W(x)$ and the expression of the Lorentz factor (11)) and

$$c_s^2(x) = \frac{1}{h(x)}\Big(\frac{\partial P}{\partial \rho}\Big|_\epsilon + \frac{x}{\rho(x)^2}\frac{\partial P}{\partial \epsilon}\Big|_\rho\Big) \tag{38}$$

Proof:

$$\frac{dF}{dx} = \frac{d}{dx}(P(\rho(x),\epsilon(x))) = \frac{\partial P}{\partial \rho}\frac{d\rho(x)}{dW}\frac{dW(x)}{dx} + \frac{\partial P}{\partial \epsilon}\Big(\frac{\partial \epsilon(x)}{\partial W}\frac{dW(x)}{dx} + \frac{\partial \epsilon(x)}{\partial x}\Big) \tag{39}$$

Each of the unknown derivatives are calculated by using the chain rule on (35),(36) and (37):

$$\begin{aligned}
\frac{d\rho(x)}{dW} &= -\frac{D}{(W(x))^2}\\
\frac{\partial \epsilon(x)}{\partial W} &= -\frac{1}{D}\Big(x + \frac{\tau + x + D}{W(x)^2}\Big) = -\frac{x}{D} - \frac{h(x)}{W(x)}\\
\frac{dW(x)}{dx} &= -\frac{v^2(x)}{h(x)}\frac{W(x)^2}{D}\\
\frac{\partial \epsilon(x)}{\partial x} &= -v^2(x)\frac{W(x)}{D}
\end{aligned}$$

where $h(x) = 1 + \epsilon(x) + x\dfrac{W(x)}{D} = \dfrac{\tau + x + D}{DW(x)}$ and $v^2(x) = \dfrac{W(x)^2 - 1}{W(x)^2}$.

Substituting in (39) and rearranging we get that

$$\frac{\partial F}{\partial x}(x) = \frac{v^2(x)}{h(x)}\Big(\frac{\partial P}{\partial \rho} + \frac{x}{\rho(x)^2}\frac{\partial P}{\partial \epsilon}\Big) \tag{40}$$

And finally we have $\dfrac{dF}{dx} = v^2(x)c_s^2(x)$. □

In order to verify the hypothesis of the fixed-point theorem we first need to determine the domain of convergence of F such that the extended variables satisfy the thermodynamical properties imposed by the EOS (13-16).

Lemma 1 *Given a phenomenological EOS (13-16) thermodynamically consistent and causal, and provided a set of conserved variables $D > 0, S, \tau > 0$, then $\mathcal{P}_{(D,S,\tau)} \neq \emptyset$.*

Proof:

Let us demonstrate that there exist a $x_{00} > 0$ such that $[x_{00}, \infty[\subset \mathcal{P}_{(D,S,\tau)}$.

Since $\lim\limits_{x\to\infty} \dfrac{|S|}{\tau + x + D} = 0$ there exist $x_{01} \geq 0$ such that $\dfrac{|S|}{\tau + x + D} < 1$, $\forall x \geq x_{01}$.

On the other hand, as $\lim\limits_{x\to\infty} W(x) = 1$ then function $\rho(x) = \dfrac{D}{W(x)}$ is increasing and bounded. Hence $\rho(x) \leq D$ and $\lim\limits_{x\to\infty} \rho(x) = D > 0$.

Considering the expression of $\epsilon(x)$, (37), its limit can be calculated as

$$\lim_{x\to\infty}\epsilon(x)=\lim_{x\to\infty}\frac{\tau+(1-W(x)^2)x+(1-W(x))D}{DW(x)}=\frac{\tau}{D}>0 \tag{41}$$

and from the definition of limit, there exists a $x_{02}\geq x_{01}$ such that for all $x>x_{02}, \epsilon(x)>0$.

From (38) let us prove that $c_s^2=\frac{\partial P(\rho(x),\epsilon(x))}{\partial\rho}\Big|_\epsilon+\frac{x}{\rho(x)^2}\frac{\partial P(\rho(x),\epsilon(x))}{\partial\epsilon}\Big|_\rho$ is non negative for the EOS under study. The partial derivatives needed are

$$\frac{\partial P(\rho(x),\epsilon(x))}{\partial\rho}\Big|_\epsilon=\left(\gamma(\rho(x))-1+\gamma'(\rho(x))\rho(x)\right)\epsilon(x)$$

and

$$\frac{\partial P(\rho(x),\epsilon(x))}{\partial\epsilon}\Big|_\rho=\left(\gamma(\rho(x))-1\right)\rho(x)$$

Then,

$$c_s^2=\frac{1}{h(x)}\left(\Big(\gamma(\rho(x))-1+\gamma'(\rho(x))\rho(x)\Big)\epsilon(x)+\frac{x}{\rho(x)^2}\Big(\rho(x)(\gamma(\rho(x))-1)\Big)\right)$$

Because of $\gamma(\rho(x))-1+\gamma'(\rho(x))\rho(x)$ is bounded and $\lim_{x\to\infty}\epsilon(x)=\frac{\tau}{D}>0$ then there exists $x_{03}\geq x_{02}$ such that for all $x\geq x_{03}$, $c_s^2\geq 0$ as the limit of the second term is infinite.

On the other hand, given the expression for the extension of the relativistic enthalpy (from (12)), $h(x)=1+\epsilon(x)+\frac{x}{\rho(x)}$, the corresponding one for the square of the relativistic sound speed is

$$c_s^2(x)=\frac{(\gamma(\rho(x))-1)(\epsilon(x)+\frac{x}{\rho(x)})+\rho(x)\gamma'(\rho(x))\epsilon(x)}{1+\epsilon(x)+\frac{x}{\rho(x)}}$$

In order to prove that this function is bounded by one we calculate the limit

$$\lim_{x\to\infty}c_s^2(x)=\frac{(\gamma(D)-1)\lim_{x\to\infty}\left(\frac{\epsilon(x)}{x}+\frac{1}{\rho(x)}\right)}{\lim_{x\to\infty}\left(\frac{1}{x}+\frac{\epsilon(x)}{x}+\frac{1}{\rho(x)}\right)}+\lim_{x\to\infty}\frac{\rho(x)\gamma'(\rho(x))\frac{\epsilon(x)}{x}}{\frac{1}{x}+\frac{\epsilon(x)}{x}+\frac{1}{\rho(x)}}=\gamma(D)-1$$

Therefore, there is a $x_{04}\geq x_{03}$ such that for $x\geq x_{04}$, $c_s^2(x)\leq\gamma(D)-1+\delta$ with $\delta>0$ and $\delta+\gamma(D)-1<1$. Then $c_s^2(x)<1$ for all $x\geq x_{04}$.

Finally, defining $x_{00}=x_{04}$, the assertion is proved. □

Corollary 1 *$F(x)$ is a non-decreasing function in $\mathcal{P}_{(D,S,\tau)}$.*

Proof: It follows from Proposition 3 and Lemma 1. □

Proposition 4 *Given a physically admissible set of conserved variables D, S, τ, there exist $a, b \in \mathcal{P}_{(D,S,\tau)}$, $a < b$, such that*

$$F([a,b]) \subset [a,b]$$

and there exists μ, $0 < \mu < 1$, associated to $[a,b]$, satisfying

$$\Big|\frac{dF(x)}{dx}\Big| \leq \mu < 1 \tag{42}$$

Therefore, $F(x)$ has a unique fixed point, x^* such that $a < x^* < b$.

Proof: We define $\mathcal{U}$ a subset of $\mathcal{P}_{(D,S,\tau)}$,

$$\mathcal{U} := \{x \in \mathcal{P}_{(D,S,\tau)} : F(x) < x\} \tag{43}$$

Let us prove that there exist $b \in \mathcal{U}$ such that $[b, \infty[\subset \mathcal{U}$ by showing that $\lim_{x\to\infty} \dfrac{F(x)}{x} = 0$. Indeed, from (41) we have that $\lim_{x\to\infty} \epsilon(x) = \dfrac{\tau}{D}$. Therefore

$$\lim_{x\to\infty} \frac{F(x)}{x} = \lim_{x\to\infty} \rho(\gamma(\rho(x)) - 1)\frac{\epsilon(x)}{x} = D(\gamma(D) - 1)\frac{\tau}{D} \lim_{x\to\infty} \frac{1}{x} = 0$$

From the definition of limit, given $\delta = 1, \exists b \in \mathcal{P}_{(D,S,\tau)}$ such that for all $x \geq b$, $\dfrac{F(x)}{x} < \delta = 1$ and then, since $F(x) > 0$, we have that $F(x) < x,\ x \in [b, \infty[$.

Because of D, S, τ is a physically admissible set of conserved variables there exists a positive $x^* > 0$ such that $x^* \in \mathcal{P}_{(D,S,\tau)}$ and $F(x^*) = x^*$.

Let us define $x^{**} = \inf \mathcal{U}$ and see that $x^* \leq x^{**}$. If $x^* > x^{**}$ then by definition of $\mathcal{U}$, $x^* \in \mathcal{U}$ and $F(x^*) < x^*$ which contradicts the hypothesis $F(x^*) = x^*$. In consequence $x^* \leq x^{**}$.

Next we show that there exist $a \in \mathcal{P}_{(D,S,\tau)}$ such that $a < x^* \leq x^{**} < b$ and $F([a,b]) \subset [a,b]$. Since F is smooth, there exist a neighborhood of x^*, $I_\delta =]x^* - \delta, x^* + \delta[$ such $I_\delta \subset \mathcal{P}_{(D,S,\tau)}$. Let us choose $a > 0$ such that $x^* - \delta < a < x^*$. Then $a < x^{**}$ and, consequently, $a \notin \mathcal{U}$ and $a \leq F(a)$. As F is an increasing function, $a \leq F(a) < F(x^{**}) = x^{**}$. Hence, using the same argument, we can show that $a \leq F(x) \leq b$ for all $x \in [a,b]$.

From Proposition 3 we have that F is differentiable in $[a,b]$ and for $x \in [a,b]$ $F'(x) = v^2(x)c_s^2(x)$.

In the following we demonstrate (42). As $x \in [a,b] \subset \mathcal{P}_{(D,S,\tau)}$ then $0 \leq v^2(x) < 1$ and $0 \leq c_s^2(x) < 1$. Therefore from Proposition 3, $0 \leq F'(x) < 1$ for all $x \in [a,b]$. On the other hand $F'(x)$ is continuous in $[a,b]$ and thus the maximum of $F'(x)$ is reached at some point $x_1 \in [a,b]$ and then

$$\mu := F'(x_1) = |F'(x_1)| = \max_{x\in[a,b]} |F'(x)| < 1$$

and $|F'(x)| \leq \mu < 1$ for all $x \in [a,b]$. Hence the fixed-point theorem can be applied so that there exists a unique fixed point in $[a,b]$, $x^* = x^{**}$, and the fixed point iterates converge to x^* starting from any initial guess $x_0 \in [a,b]$. □

Remark 1 The case of the ideal gas EOS, $P(\rho,\epsilon)=(\gamma-1)\rho\epsilon$ with γ constant, if x is such that $v^2(x)<1$ and $\epsilon(x)>0$ then $c_s^2(x)=\dfrac{(\gamma-1)\left(\epsilon(x)+\dfrac{x}{\rho(x)}\right)}{1+\epsilon(x)+\dfrac{x}{\rho(x)}}\leq\gamma-1<1$. Therefore $\mu=\gamma-1$ and the obtained pressure x^* is causal.

In the following we provide the necessary and sufficient condition to ensure convergence of the fixed-point iterative procedure. To this end we use a relevant result by Wu and Tang in [44] (see also [45,46]) that following our notation is expressed in the following Lemma.

Lemma 2 *Let* $\mathcal{A}=\{(D,S,\tau):\epsilon=\frac{\tau+P+D}{D+W}-\frac{PW}{D}-1>0,\rho=\frac{D}{W},P>0,$ *and* $|v|=\frac{|S|}{\tau+P+D}<1\}$ *with* $P=P(\rho,\epsilon)$ *an equation of state satisfying*

$$h\geq\sqrt{1+\frac{P^2}{\rho^2}}+\frac{P}{\rho}\qquad where\qquad h=1+\epsilon+\frac{P}{\rho}$$

Then, if $(D,S,\tau)\in\mathcal{A}$ *we have that*

$$D>0\ and\ \tau+D\geq\sqrt{D^2+S^2}$$

Proof: See Lemma 3.1 in ([44]).□

Proposition 5 *Given a phenomenological EOS defined through (13-16) which is thermodynamical consistent and causal, the inequality*

$$h\geq\sqrt{1+\frac{P^2}{\rho^2}}+\frac{P}{\rho}\qquad where\qquad h=1+\epsilon+\frac{P}{\rho}\qquad is\ satisfied.$$

Proof: Using the definition of h the inequality shows as

$$1+\epsilon+\frac{P}{\rho}\geq\sqrt{1+\frac{P^2}{\rho^2}}+\frac{P}{\rho}$$

which is equivalent to $1+\epsilon\geq\sqrt{1+\frac{P^2}{\rho^2}}$. We prove the latter.

Since $P=(\gamma-1)\rho\epsilon$ we can define $g(\epsilon)=1+\epsilon-\sqrt{1+(\gamma-1)^2\epsilon^2}$. Then we have that $g(0)=0$ and, since $\gamma-1\leq1$,

$$g'(\epsilon)=1-(\gamma-1)\frac{(\gamma-1)\epsilon}{\sqrt{1+(\gamma-1)^2\epsilon^2}}\geq0$$

Hence, $g(\epsilon)\geq0$ for all $\epsilon\geq0$ and therefore the inequality is satisfied. □

Lemma 3 *Given a phenomenological EOS defined through (13-16) which is thermodynamical consistent and causal and given a triple* $(D,S,\tau)\in\mathcal{A}$ *(as in Lemma 2), then*

$$F(0)>0$$

Proof: Given a triple (D, S, τ) from Lemma 2 we have that

$$D > 0 \text{ and } \tau + D \geq \sqrt{D^2 + S^2}$$

Since $\tau + D \geq \sqrt{D^2 + S^2} > \sqrt{S^2}$ then $|S| < \tau + D$ and therefore $v(0) = \frac{S}{\tau + D}$ and $|v(0)| < 1$. Hence $W(0) = \frac{1}{\sqrt{1-u(0)^2}} \geq 1$ and $\rho = \frac{D}{W(0)} > 0$.

Since $F(x) = P(\rho(x), \epsilon(x)) = (\gamma(\rho(x)) - 1)\rho(x)\epsilon(x)$ then we have yet to prove that $\epsilon(0) > 0$.

Indeed, since $\epsilon(x) = \frac{\tau + x + D}{D + W(x)} - \frac{xW(x)}{D} - 1$ (equation (37)), $\epsilon(0) = \frac{\tau + D}{D + W(0)} - 1$. The value of $W(0)$ is obtained from

$$W(0) = \frac{1}{\sqrt{1 - \frac{S^2}{(\tau + D)^2}}} = \frac{\tau + D}{\sqrt{(\tau + D)^2 - S^2}}.$$

Since the function $g(z) = \frac{z}{\sqrt{z^2 - S^2}}$ is monotonically decreasing because $g'(z) = \frac{-S^2}{(z^2 - s^2)^{3/2}} < 0$ then, using $\tau + D > \sqrt{D^2 + S^2}$ we have

$$W(0) = g(\tau + D) < g(\sqrt{D^2 + S^2}) = \sqrt{1 + \left(\frac{S}{D}\right)^2}$$

On the other hand

$$\epsilon(0) = \frac{\tau + D}{DW(0)} - 1 > \frac{\sqrt{D^2 + S^2}}{D} \frac{1}{\sqrt{1 + \left(\frac{S}{D}\right)^2}} - 1 = 0$$

Thus, $\epsilon(0) > 0$ and $F(0) > 0$. □

Theorem 1 *Given a phenomenological EOS defined through (13-16) which is thermodynamical consistent and causal and given a triple $(D, S, \tau) \in \mathcal{A}$ (as in Lemma 2), if $x^0 \geq 0$ is chosen as initial guess then the fixed point iteration $x^{k+1} = F(x^k)$ converges monotonically to the unique value of the pressure $P^* := x^*$, $F(x^*) = x^*$.*

Proof: From Proposition 5 and Lemma 3 we have that $F(0) > 0$. Then, if the subset $\mathcal{U}$ is defined as in (43)

$$\mathcal{U} := \{x \in \mathcal{P}_{(D,S,\tau)} : F(x) < x\}$$

we have that $0 < \inf \mathcal{U}$ and therefore $0 < x^* = \inf \mathcal{U}$ is a fixed point of F.
Let $x^0 \geq 0$. From Corollary 1 we have that F is a strictly increasing function. If $x^0 > x^* = \inf \mathcal{U}$ the sequence of iterates is strictly decreasing, $x^0 > x^1 > \cdots > x^k > \cdots > x^*$, and converges to x^*. On the other hand, if $0 \leq x^0 < x^*$ the sequence $x^k = F(x^{k-1})$ is strictly increasing and converges to x^*.

From Proposition 4 we have that the fixed point is unique. Then, the iterates $x^{k+1} = F(x^k)$ starting with any $x^0 \geq 0$ converge to x^*. □

The fixed-point iteration discussed above ensures linear convergence to calculate the fixed-point α of F such that $F(\alpha) = \alpha$. Next we propose a Newton type iterative procedure to explore quadratic convergence for the recovery of primitive variables.

3.2.2 Newton's iteration

Our Newton iteration to recover primitive variables in each time step of the evolution of SRHD equations consists of applying Newton's method to the function $F(x) - x$ where $F(x)$ is defined as in the previous section (Definition 1). The Newton iteration function is then

$$N(x) = x - \frac{F(x) - x}{F'(x) - 1} \tag{44}$$

and is well defined since $0 < F'(x) < 1$ as $F(x)$ satisfies Lemma 1.

The Newton iterative procedure to recover the value of the pressure as fixed point of the iteration is then

$$x^{k+1} = x^k - \frac{F(x^k) - x^k}{F'(x^k) - 1} \tag{45}$$

for $k = 0, 1, \cdots$ given as initial x^0 an estimated value of the pressure.

We analyze the convergence of iteration (45) for the case where the pressure is defined through the phenomenological EOS (13-16). In order to establish the conditions to ensure quadratic convergence we examine the general result by Kantorovich on convergence of Newton's iterative procedure characterized in the following Theorem [34].

Kantorovich's Theorem *(on Newton's method for real-valued functions) Let* $]a, b[, a < b$ *be an open interval in* $\mathcal{R}$*. Assume* $f(x) :]a, b[\rightarrow \mathcal{R}$ *is a continuous function which is twice differentiable such that the second derivative is bounded, i.e., there is a constant* $K > 0$ *such that* $|f''(x)| \leq K$ *for all* $x \in]a, b[$*. Let* $x^0 \in]a, b[$ *be a pivot such that* $|f'(x^0)| \neq 0$ *and*

$$\eta = \frac{|f(x^0)|}{|f'(x^0)|}$$

satisfies that

$$\frac{K\eta}{|f'(x^0)|} < \frac{1}{2}$$

Then, the Newton iterates

$$x^{k+1} = x^k - \frac{f(x^k)}{f'(x^k)}$$

are well defined and converge quadratically to a point x^* *such that* $f(x^*) = 0$ *where* $x^* \in]a, b[$.

Following Kantorovich's Theorem we study the convergence of iteration (45), $x^{k+1} = N(x^k)$, applying Newton's method to $f(x) = F(x) - x$ starting from a pivot x^0 satisfying Kantorovich conditions.

In order to analyze the convergence we need the derivative of $N(x)$,

$$N'(x) = \frac{F(x) - x}{(F'(x) - 1)^2} F''(x) \tag{46}$$

as well as an expression for $F''(x)$ which is derived in the following Proposition. We assume F is defined in the domain and under conditions established in Lemma 1.

Proposition 6 *Given an EOS, $P = P(\rho, \epsilon)$, and a set of conserved variables $D > 0, S$ and $\tau > 0$ we have functions $v^2(x), h(x)$, and $c_s^2(x)$ defined for $x > 0$. Then*

$$F''(x) = \frac{d}{dx}\Big(v^2(x)c_s^2(x)\Big) = \frac{2v^2(x)c_s^2(x)}{h(x)}\,\frac{W(x)}{D}\Big(v^2(x)\mathcal{G}(x) - \frac{3}{2}\Big) \tag{47}$$

where $\mathcal{G}$ is the extension of the fundamental derivative to the domain $x > x_{00}$,

$$\mathcal{G}(x) = 1 + \frac{\rho(x)}{2a^2(x)}\left(\frac{\partial a^2}{\partial \rho}(x) + \frac{x}{\rho(x)^2}\frac{\partial a^2}{\partial \epsilon}(x)\right) \tag{48}$$

and $a^2(x) = \frac{\partial P}{\partial \rho}\Big|_s(\rho(x), \epsilon(x))$, s entropy.

Proof:

$$\begin{aligned}\frac{d}{dx}\Big(v^2(x)c_s^2(x)\Big) &= \frac{d}{dx}\Big(v^2(x)\frac{a^2(x)}{h(x)}\Big)\\ &= v^2(x)\frac{h(x)\frac{da^2(x)}{dx} - a^2(x)\frac{dh(x)}{dx}}{h(x)^2} + \frac{a^2(x)}{h(x)}\frac{dv^2(x)}{dx}\end{aligned}$$

In order to complete this calculation we need the following derivatives

$$\frac{da^2(x)}{dx} = \frac{v^2(x)}{h(x)}\Big(\frac{\partial a^2}{\partial \rho}(x) + \frac{x}{\rho(x)^2}\frac{\partial a^2}{\partial \epsilon}(x)\Big) = \frac{v^2(x)}{h(x)}\,2\frac{a^2(x)}{\rho(x)}(\mathcal{G}(x) - 1) \tag{49}$$

$$\begin{aligned}\frac{dh(x)}{dx} &= \frac{W(x)}{D}\\ \frac{dv^2(x)}{dx} &= -\frac{v^2(x)}{h(x)}\,\frac{2}{DW(x)}\end{aligned}$$

Substituting and rearranging, expression (47) is obtained.□

The expression of the second derivative of $F(x)$ indicates dependence of $N'(x)$ on the non-convex - thermodynamically - region through the value of the fundamental derivative $\mathcal{G}$. Let us explore how much influence this dependence on the thermodynamics has on the convergence of Newton's iteration.

Proposition 7 *Given a thermodynamically consistent and causal phenomenological EOS of type (13-16) and given a set of physically admissible conserved variables there exists a neighborhood of the fixed point of $F(x)$, $x^* > 0$, such that Newton's method converges.*

Moreover, there exists a pivot $x_0 \in \mathcal{P}_{(D,S,\tau)}$ such that the sequence of iterates converges quadratically to the fixed point x^*.

Proof: Given a set of physically admissible conserved variables we have, by Proposition 4, that there exists $[a, b] \subset \mathcal{P}_{(D,S,\tau)}$ such that the fixed point of F, x^*, is in $]a, b[$.

By Proposition 5, $\mathcal{G}$ is C^2 in $\mathcal{P}_{(D,S,\tau)}$ and therefore F'' is bounded in $[a, b]$ so that there exists $K > 0$ such that $|F''(x)| \leq K$, $\forall x \in [a, b]$.

From (47) it follows that for $x \in [a, b]$,

$$|F''(x)| \leq \frac{2W(a)}{D}\left(|\mathcal{G}| + \frac{3}{2}\right) \tag{50}$$

The maximum of $|\mathcal{G}|$ is reached in the set $G = \{x : 0 < \rho(x) < \rho_1 + 2\sigma\}$. We denote by

$$M = \max_{x \in G} |\mathcal{G}| > 0$$

and then (50) can be bounded by

$$K = \frac{2W(a)}{D}\left(M + \frac{3}{2}\right)$$

Hence, under these conditions we can assert that there is a neighborhood of x^* such that Newton's method converges.

On the other hand, by Proposition 4, given $x_0 \in [a, b]$ the fixed point iteration $x^{k+1} = F(x^k)$, $k = 0, 1, \cdots$ converges to x^* and $0 \leq |F'(x^k)| \leq \mu < 1$ is satisfied. Then there is an iterate k_0, $x^{k_0} \in [a, b]$, such that

$$|F(x^{k_0}) - x^{k_0}| < \frac{1}{2}\frac{1}{K}(F'(x^{k_0}) - 1)^2$$

Thus

$$\frac{K|F(x^{k_0}) - x^{k_0}|}{(F'(x^{k_0}) - 1)^2} < \frac{1}{2} \tag{51}$$

We can use Newton method choosing x^{k_0} as initial guess and by Kantorovich theorem we will reach quadratic convergence. □

Proposition 7 provides a sufficient condition to guarantee quadratic convergence of the Newton's iteration for recovering primitive variables in the evolution of SRHD equations closed with any EOS. The efficiency in the convergence depends, in principle, on the good choice of the pivot x^0. However, condition (51) and the definition of the second derivative (47) indicate that the constraint is stiffer when the EOS is non-convex. The second derivative of F might reach large values in the neighborhood of the boundary of the non-convex region (points where the fundamental derivative $\mathcal{G}$ changes sign). In those cases, the convergence of the iteration is compromised and the closer to the solution is x^{k_0}, the better to fulfill the constraint (51).

The speed of convergence of the fixed-point method is related with the one of Newton's method. The linear convergence of the fixed-point method is slow if $F'(x)$ is close to 1, and the increment of the Newton's iterate includes as denominator $|F'(x) - 1|$ then the Newton sequence converges slowly outside the region of quadratic convergence

Taking all this analysis into consideration we propose a practical criterion to follow in the process of recovering primitive variables.

Practical criterion for primitive variable recovering

Our strategy combines both methods, the fixed-point (33-37) and the Newton iteration (45). This consists of calculating few k_0 iterates of the fixed-point iteration $x^k = F(x^{k-1})$ starting with any $x^0 \geq 0$ (Theorem 1) such that x^{k_0} satisfies the hypothesis of the Kantorovich Theorem, i.e., it is close enough to the exact

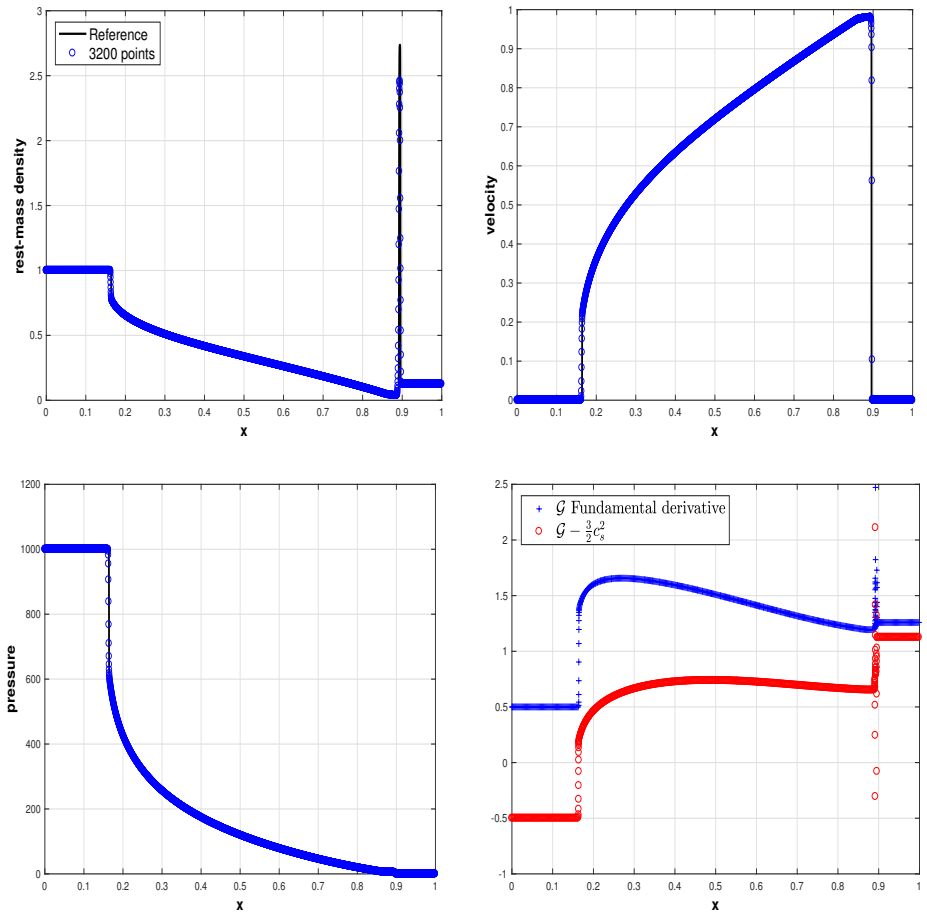

Fig. 3 Rest-mass density, velocity, pressure, fundamental derivative and relativistic nonlinearity term profiles for the relativistic blast wave with data parameters for EOS1.

root. Then, we use x^{k_0} as the initial guess of the Newton iteration and compute a couple of iterations which will be sufficient to reach double precision accuracy as quadratic convergence is ensured.

In the scenarios where a very small fixed point ($x^* << 1$) is expected (i.e. pressure values close to zero) we can use $x^0 = 0$ as initial guess to ensure efficient monotonic convergence of the fixed point interation.

In addition, as a rule of the thumb, starting with a guess equal to zero, $x^0 = 0$, allows us to validate whether a given triple is admissible. Indeed, if the first iterate of the fixed point iteration was not positive (i.e. $F(0) \leq 0$) then the given triple is not admissible.

4 Numerical examples

The study of Riemann problems - initial valued problems with data consisting of two constant states- allows to understand the anomalous dynamics developed

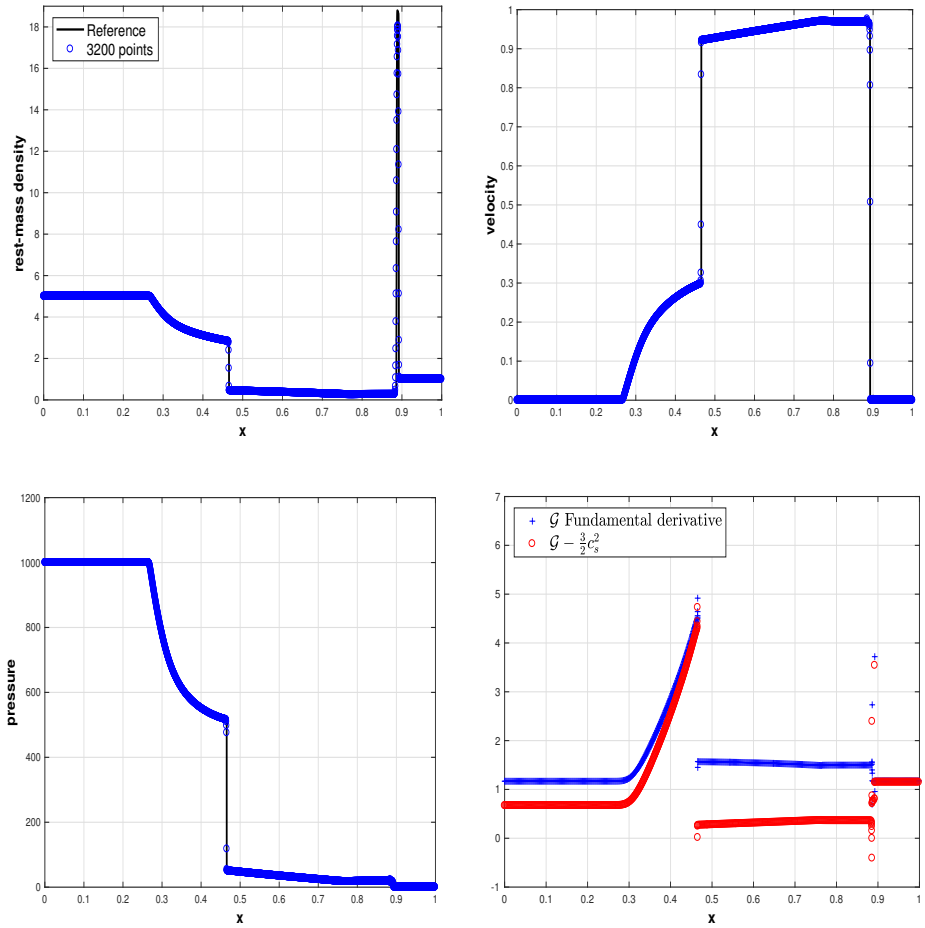

Fig. 4 Rest-mass density, velocity, pressure, fundamental derivative and relativistic nonlinearity term profiles for the relativistic blast wave with data parameters for EOS2.

by non-convex hyperbolic system of conservation laws. The impact of non-convex EOS on the wave structure of the hyperbolic system of classical hydrodynamics by means of the study of Riemann problems has been widely investigated in the literature ([31]).

We present a set of relativistic Riemann problems that have been designed to exhibit non-classical dynamics in the relativistic regime. We consider the phenomenological EOSs defined from (13-16) with the two set of parameters in Table 1 guaranteeing causality and thermodynamical consistency.

We show the evolution of two blast waves, one with genuinely relativistic non-classical dynamics and another where the complex wave structure is induced because of the flow enters into a non-convex - thermodynamically - region, due to relativistic effects (change of sign of $\mathcal{G}$). We also show the evolution of two relativistic expanding slabs and two relativistic colliding slabs. The initial data of the Riemann problems are displayed in Table 2. For each problem we plot the

Table 2 Initial Data of Riemann problems

	ρ_L	v_L	p_L	ρ_R	v_R	p_R
Blast Wave EOS1	1.0	0	1000	0.125	0	0.01
Blast Wave EOS2	5	0	1000	0.125	0	0.01
Expanding Slabs EOS1	10	-0.9	10	10	0.9	10
Colliding Slabs EOS2	0.05	0.999	0.05	0.05	-0.999	0.05

profiles of the rest-mass density, velocity, pressure, fundamental derivative $\mathcal{G}$ and relativistic nonlinearity term (29) at time $t = 0.4$ of the evolution.

Both blast waves evolutions showed in Figure 3 and Figure 4 share an initial jump of five orders of magnitude in pressure causing the formation of two highly dense and extremely thin shells. As typical in blast waves scenarios the shells are approximated as a lead shock wave and a contact discontinuity.

Figure 3 displays the evolution of the first blast wave data set with EOS1. The initial data have been chosen so the left state belongs to the genuine relativistic non-convex region, i.e., the nonlinearity term (29) is negative, $\nu(\rho_L, \epsilon_L) = \mathcal{G}(\rho_L) - \frac{3}{2}c_s^2(\rho_L, \epsilon_L) < 0$ while $\mathcal{G}(\rho_L) > 0$. The right state belongs to the classical convex region ($\nu(\rho_R, \epsilon_R) > 0$).

The path connecting both states after time 0.4 consists of the thin shell propagating to the right and a composite wave expanding to the left formed by an expansive rarefaction attached to a shock. The composite wave can be clearly observed in the velocity and pressure profiles. The picture at the bottom right shows how the fundamental derivative is positive in the whole domain while relativistic effects provoke negative values of the nonlinearity term $\nu(\rho, \epsilon)$.

Figure 4 shows the evolution of the second blast wave data set with EOS2. The strong relativistic blast wave presents a very high density shell and a composite wave moving to the left formed by two rarefaction waves joined through a shock wave. The rarefaction-shock-rarefaction structure is nicely depicted in the velocity profile. The non-classical wave structure is due mainly to the fact that the flow enters into a non-convex - thermodynamically - region, due to relativistic effects (change of sign of the fundamental derivative). Both thin shock towers in either blast wave exemplify two examples of hard tests for any numerical scheme.

Figure 5 presents the result of evolving the initial data of two expanding slabs with EOS1. In this case, the initial data corresponds to a state with two gases at constant density and pressure expanding away from each other with a speed equal to 0.9. The left and right states belong to the convex region, $\nu(\rho_{L,R}, \epsilon_{L,R}) > 0$. The initial velocities are prescribed with the same magnitude and opposite sign in order to expand the two gases in opposite directions, so that the two fluid streams evacuate the central region of the computational domain, with respect to which, the solution is symmetric. The path connecting both states crosses the region where the relativistic nonlinearity term $\nu(\rho, \epsilon)$ is negative. The wave structure consists of two composite waves traveling from the center in opposite directions. Each of the two composite waves consists of three pieces: two rarefaction waves connected through a shock wave. Similarly as in previous examples, the profile of the fundamental derivative and relativistic nonlinearity factor show the regions where the complex structure is developed.

The evolution of two colliding slabs with EOS2 is plotted in Figure 6. Initial data of density and pressure are identical at both side states while the velocity is

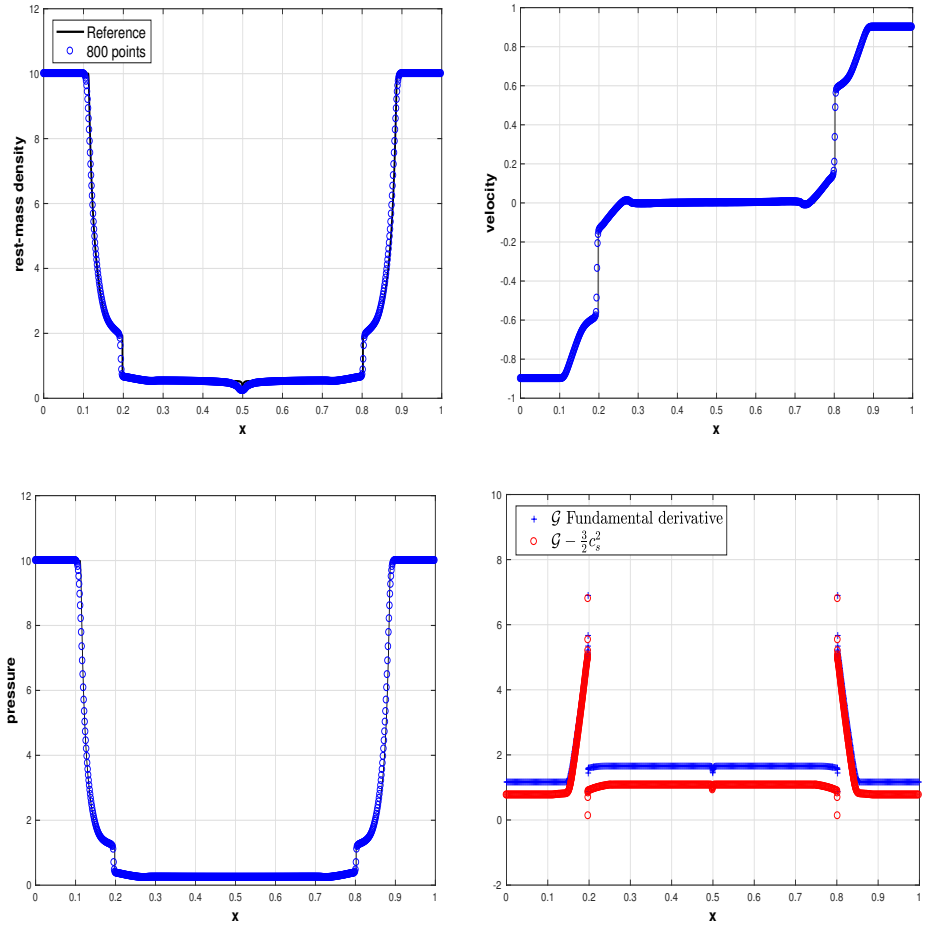

Fig. 5 Rest-mass density, velocity, pressure, fundamental derivative and relativistic nonlinearity term profiles for the expanding slabs example with data parameters for EOS1.

such that the two gases hit each other with opposite and equal speeds of 0.999. The values are chosen such that the left and right states belong to the convex region. As in the previous case the path connecting both states crosses the region where the relativistic nonlinearity term $\nu(\rho, \epsilon)$ is negative. The complex wave structure consists of two composite waves formed by two shocks separated by a compression wave. Both composites travel in opposite directions.

4.1 Two dimensional examples

The extension to higher dimensions is accomplished in a dimension by dimension fashion as in ([39,37]). We present examples in the $[0,1] \times [0,1]$ domain using the two dimensional third order accurate version of our code under CFL= 0.4.

As a test we evolve a two dimensional version of the one dimensional blast wave with EOS1 in a 45 degree rotated coordinates. The Riemann data are prescribed

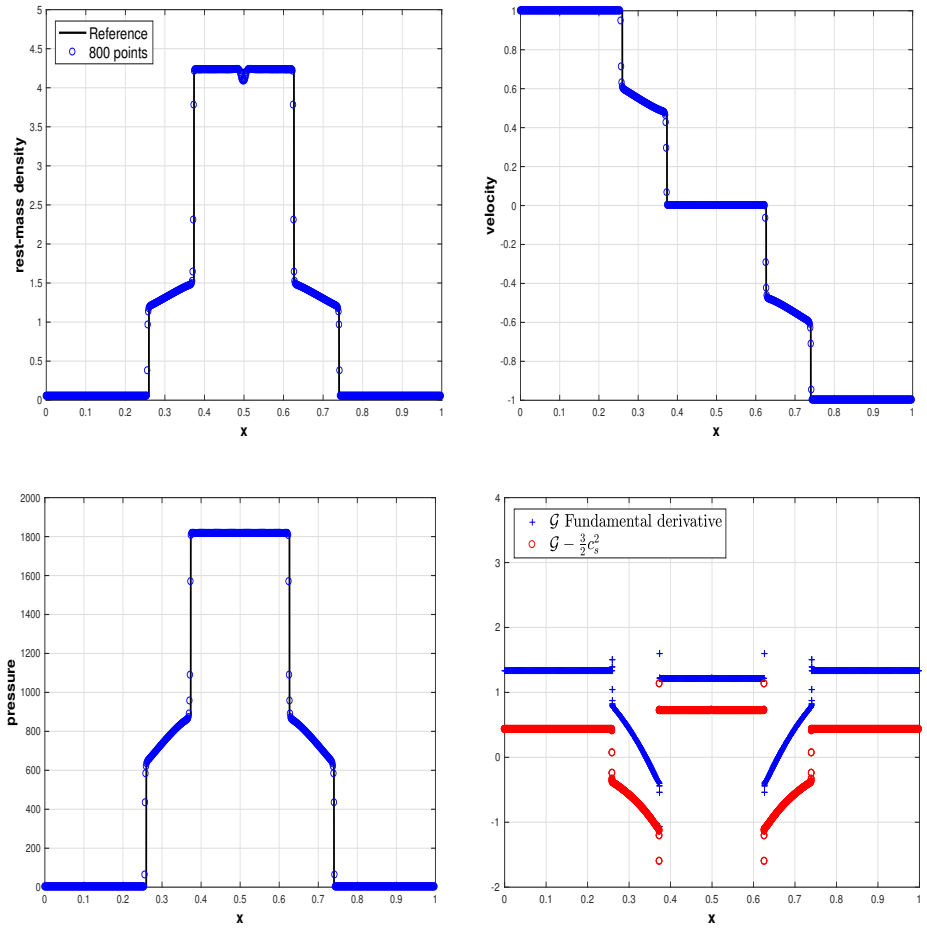

Fig. 6 Rest-mass density, velocity, pressure, fundamental derivative $\mathcal{G}$ and relativistic nonlinearity term profiles for the colliding slabs example with data parameters for EOS2.

initially at both sides of the diagonal. We compute with a 800×800 grid until time $0.4 \cdot \sqrt{2} \approx 0.5656$. Figure 7 shows a diagonal cut of the computed quantities of the rest-mass density and the magnitude of the velocity compared with a reference solution obtained through the one dimensional version of our code with 12800 points. We observe that the complex wave structure is captured as expected.

We examine a Riemann problem for two dimensional relativistic gas. Two dimensional Riemann problems have been introduced in [40] for Newtonian hydrodynamics with ideal EOS. These involve the interactions of elementary waves as shocks, rarefactions or contact discontinuities initially separated by constant states. We consider the extension to relativistic flows of a two dimensional Riemann problem presented in [9,33]. The initial data are constant in each quadrant

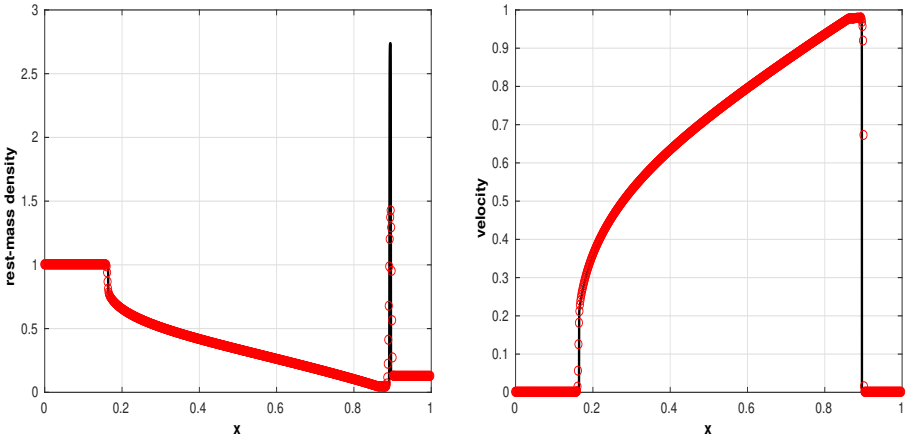

Fig. 7 Two-dimensional diagonal Riemann problem. Rest-mass density and velocity profiles for the relativistic blast wave with data parameters for EOS1.

and involve two shocks and two tangential discontinuities.

$$(\rho, v_x, v_y, P) = \begin{cases} (0.1, 0, 0, 0.01); & x \geq 0.5, \ y \geq 0.5 \\ (0.1, 0.99, 0, 1); & x < 0.5, \ y \geq 0.5 \\ (0.5, 0, 0, 1); & x < 0.5, \ y < 0.5 \\ (0.1, 0, 0.99, 1); & x \geq 0.5, \ y < 0.5 \end{cases}$$

Figure 8 shows the density logarithms at time $t = 0.4$ with the ideal EOS with $\gamma = 5/3$ (left) and with the phenomenological EOS2 (right). The results are computed with a 400×400 grid. We use the same computational setting in both simulations. In both cases we observe the expected structure. The complex flow contains two curved shocks in first quadrant symmetric with respect to the diagonal and a jet-like structure moving along the third quadrant. The curvature of the shocks is larger for the non-convex case. The morphological differences are due to the thermodynamics induced by the respective EOS.

5 Conclusions

We present a numerical method for the approximation of the complex wave structure arising in the solution of special relativistic hydrodynamics closed with non-convex EOSs. We consider a class of non-convex phenomenological Mie-Grüneissen EOSs and settle the conditions under which the EOS is causal and thermodynamically consistent to ensure hyperbolicity of the system of equations. The numerical method approximates the numerical fluxes following an upwind characteristic based approach. The method is low dissipative and is able to detect regions where complex wave structure is generated. We analyze two iterative procedures to recover primitive variables in each time step of the evolution and demonstrate their convergence in terms of the thermodynamical variables playing an important role in the formation of complex dynamics. We design an efficient strategy based on the iterative procedures and prove that convergence is ensured when selecting a non-negative initial guess. We propose a set of Riemann problems showing strong and

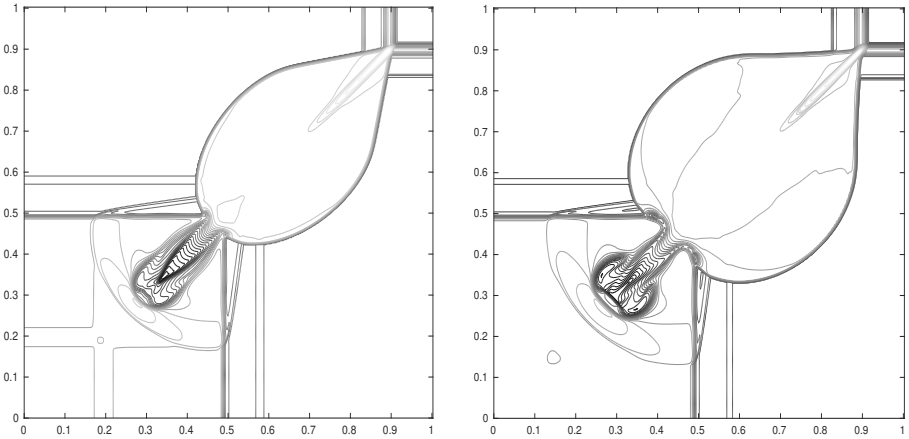

Fig. 8 Density logarithms for the two dimensional Riemann problem at time t=0.4. Left picture represents results with Ideal EOS and gamma 5/3. Right picture represent results with the phenomenological EOS2

complex wave structures in the relativistic regime. The examples display composite waves formed as a result of a non-convex dynamics induced by the non-convex EOS as well as complex wave structures resulting from non-convex relativistic effects.

6 Acknowledgments

The authors would like to thank the referees for their valuable comments and recommendations which helped to improve the manuscript.

Work partially supported by the Spanish Government grants: PGC2018-101119-B-100 and PGC2018-095984-B-100; and the local Autonomous Government of the Valencia's Community grant PROMETEO-2014-069.

References

1. Aloy, M.A., Ibáñez, J.M., Sanchis-Gual, N., Obergaulinger, M., Font, J.A., Serna, S., Marquina, A., Neutron star collapse and gravitational waves with a non-convex equation of state, MNRAS, 484, 4980-5008, 2019.
2. Anile, A.M., Relativistic Fluids and Magneto-Fluids, Cambridge Univ. Press, Cambridge, 1989.
3. Argrow, B.M., Computational analysis of dense gas shock tube flow, Shock Waves 6:241-248, 1996.
4. Bauswein, A., Janka, H.-T. and Oechslin, R., Phys.Rev.D, vol. 82, 084043, 2010.
5. Bethe, H.A., The theory of shock waves for an arbitrary equation of state, Technical Report 545 Office of Scientific Research and Development 1942.
6. Brio, M., Wu, C.C., An upwind differencing scheme for the equations of ideal magnetohydrodynamics J. Comput. Phys., 75, 2, 400-422, 1988.
7. Cinnella P., Corre C., in APS Division of Fluid Dynamics Meeting Abstracts, 2006.
8. Cinnella P., Phys.Fl, vol 20, 046103, 2008.
9. Del Zanna,L and Bucciantini, N, An efficient shock-capturing central-type scheme for multidimensional relativistic flows, A&A, 390,1177, 2002.

10. Donat R and Marquina,A Capturing Shock Reflections: An improved Flux Formula, J. Comput. Phys. 125, 42-58, 1996.
11. Donat R, Font JA, Ibáñez, JM, Marquina, A, A Flux-Split algorithm applied to relativistic flow, J. Comput. Phys, 146, 58-81, 1998.
12. J Font, J.A., Ibáñez, J.M., Marquina, A., Martí, J.M., Astron. Astrophys., 282, p. 304, 1994.
13. Guardone, A. and Vigevano,L. , Roe Linearization for the van der Waals Gas, J. Comp. Phys. 175, 50-78, 2002.
14. Guardone, A. and Zamfirescu, C. and Colonna, P., Maximum intensity of rarefaction shock waves for dense gases, J. Fluid Mech., 642, 127, 2010
15. Haensel, P., Levenfish, K. P., Yakovlev, D. G., Astronomy and Astrophysics, vol. 394, 213, 2002.
16. Haensel, P., Potekhin, A. Y., Astronomy and Astrophysics, vol. 428, 191, 2004.
17. Haensel, P., Potekhin, A. Y., Yakovlev, D. G., eds, Neutron Stars 1 : Equation of State and Structure, Astrophysics and Space Science Library Vol. 326, 2007.
18. Heuze, O, Jaouen, S, Jourdren, H, Dissipative issue of high-order shock capturing schemes with non-convex equations of state, J. Comp. Phys 228, 833-860, 2009.
19. Ibáñez, J. M., Cordero-Carrión, I. and Martí, J. M. and Miralles, J. A.,On the convexity of relativistic hydrodynamics, Classical and Quantum Gravity, 30, 057002, 2013.
20. Ibáñez, J.M., Marquina, A., Serna, S., Aloy, M.A., Anomalous dynamics triggered by a non-convex equation of state in relativistic flows,MNRAS, 476, 1100, 2018.
21. Janka H.-T., Hanke F., Hüdepohl L., Marek A., Müller B., Obergaulinger M., Progress of Theoretical and Experimental Physics, 01A309, 2012.
22. Lax, PD, Hyperbolic systems of conservation laws and the mathematical theory of shocks waves, SIAM, Philadelphia, 1973.
23. LeVeque RJ, Mihalas, D, Dorfi, EA, Müller, E, Computational methods for astrophysical fluid flow, Saas-Fee Advanced Courses, 27, Springer-Verlag, New York, 1998.
24. LIGO Scientific Collaboration and Virgo Collaboration, GW170817: Observation of Gravitational Waves from a Binary Neutron Star Inspiral, Phys.Rev.Letters, vol. 119, 161101, 2017.
25. Martí J. M., Miralles J. A., Ibanez J. M., Diaz-Alonso J., Astroph. Journal , 329, 780, 1988
26. Martí, J. M. and Müller, E., *Numerical Hydrodynamics in Special Relativity*, Living Rev. Relativ. 6: 7. https://doi.org/10.12942/lrr-2003-7, 2003.
27. Martí, J. M. and Müller, E., *Grid-based Methods in Relativistic Hydrodynamics and Magnetohydrodynamics*, Living Rev. Comput. Astrophys. 1: 3. https://doi.org/10.1007/lrca-2015-3, 2015.
28. Martí, J.M., Müller, E., Font, J.A., Ibáñez, J.M., Marquina, A., *Morphology and dynamics of relativistic jets*, Astroph. Journal, 479, 1,151, 1997.
29. Marquina, A., Martí, J.M., Ibáñez, J.M., Miralles, J.A., Donat, R., Astron. Astrophys., 258, p. 566, 1992.
30. Marquina, A., *Local piecewise hyperbolic reconstructions for nonlinear scalar conservation laws*, SIAM J. Sci. Comp. 15,892-915, 1994.
31. Menikoff, R., *Empirical Equations of State for solids*, in: ShockWave Science and Technology Reference Library Eds. Horie, Yasuyuki, Springer Berlin Heidelberg, 143-188, 2007.
32. Menikoff, R. and Plohr, B.J., *The Riemann problem for fluid flow of real materials*, Rev. Mod. Phys. , Vol. 61, No. 1, 1989.
33. Mignone, A., and Bodo, G., A HLLC Riemann solver for relativistic flows-I. Hydrodynamics, MNRAS, 364, 126-136, 2005
34. Ortega J.M., Rheinbolt, W.C., Iterative solution of nonlinear equations in several variables, Academic Press NY, 1970.
35. Rezzolla, L. and Zanotti, O., Relativistic Hydrodynamics, Oxford University Press, 2013.
36. Serna, S., Marquina A., Capturing shock waves in inelastic granular gases , J. Comput. Phys., 209, 2, 787-795, 2005.
37. Serna, S., A characteristic-based nonconvex entropy-fix upwind scheme for the ideal magnetohydrodynamic equations, J.Comput. Phys, 228, 4232-4247, 2009.
38. Serna, S., Marquina A., Anomalous wave structure in magnetized materials described by non-convex equations of state, Phys. Fluids, 26, 016101, 2014.
39. Shu, C.W., Osher, S. Efficient implementation of essentially non-oscillatory shock-capturing schemes, 2, J. Comput. Phys., 83, 1, 32-78, 1989.

40. Schulz-Rinne,C.W., Collins, J.P., Glaz, H.M., Numerical Solution of the Riemann Problem of Two-Dimensional Gas Dynamics, SIAM J. Sci. Comput, 14, 1394-1414,1993
41. Thompson, P. A., A Fundamental Derivative of Gas Dynamics, Phys. Fluids,14,1843-1849,1971.
42. Voss A., PhD thesis, University of Wuppertal, 2005.
43. Wu, K., Tang, H., *High-order accurate physical-constraints-preserving finite difference WENO schemes for special relativistic hydrodynamics*, J. Comp. Phys., 298, 539-564, 2015.
44. Wu, K., Tang, H., *Physical-constraint-preserving central discontinuous Galerkin methods for special relativistic hydrodynamics with a general equation of state*, Ap. J. Suppl., 228:3 (23pp), 2017.
45. Wu, K., *Design of provably physical-constraint-preserving methods for general relativistic hydrodynamics*, Phys. Rev. D, 95, 103001, 2017.
46. Wu, K., Tang, H., *Admissible states and physical-constraints-preserving schemes for relativistic magnetohydrodynamic equations*, Math. Models Methods Appl. Sci., 27, 1871-1928, 2017.
47. Zeldovich Y., Zh. Eksp. Teor. Fiz., 4, 363, 1946.